

Changing sources and processes sustaining surface CO₂ and CH₄ fluxes along a tropical river to reservoir system

Cynthia Soued¹, Yves T. Prairie¹

¹Groupe de Recherche Interuniversitaire en Limnologie et en Environnement Aquatique (GRIL), Département des Sciences
5 Biologiques, Université du Québec à Montréal, Montréal, H2X 3X8, Canada.

Correspondence to: Cynthia Soued (cynthia.soued@gmail.com)

Abstract. Freshwaters are important emitters of carbon dioxide (CO₂) and methane (CH₄), two potent greenhouse gases (GHG). While aquatic surface GHG fluxes have been extensively measured, there is much less information about their underlying sources. In lakes and reservoirs, surface GHG can originate from horizontal riverine flow, the hypolimnion, littoral
10 sediments, and water column metabolism. These sources are generally studied separately, leading to a fragmented assessment of their relative role in sustaining CO₂ and CH₄ surface fluxes. In this study, we quantified sources / sinks of CO₂ and CH₄ in the epilimnion along a hydrological continuum in a permanently stratified tropical reservoir (Borneo Island). Results showed that horizontal inputs are an important source of both CO₂ and CH₄ (> 90 % of surface emissions) in the upstream reservoir branches. However, this contribution fades along the hydrological continuum, becoming negligible in the main basin of the
15 reservoir, where CO₂ and CH₄ are uncoupled and driven by different processes. In the main basin, vertical CO₂ inputs and sediment CH₄ inputs contributed to on average 60 and 23 % respectively to the surface fluxes of the corresponding gas. Water column metabolism exhibited wide amplitude and range for both gases, making it a highly variable component, but with a large potential to influence surface GHG budgets in either direction. Overall our results show that sources sustaining surface CO₂ and CH₄ fluxes vary spatially and between the two gases, with internal metabolism acting as a fluctuating but key
20 modulator. However, this study also highlights challenges and knowledge gaps related to estimating ecosystem-scale CO₂ and CH₄ metabolism, which hinder aquatic GHG flux predictions.

1 Introduction

Surface inland waters are globally significant sources of greenhouse gases (GHG) to the atmosphere, namely carbon dioxide
25 (CO₂) and methane (CH₄) (Bastviken et al., 2011; DelSontro et al., 2018a; Raymond et al., 2013). Freshwaters act as both transport vessels for terrestrial carbon (C) and as active biogeochemical processors, making them key sites of GHG exchange with the atmosphere (Tranvik et al., 2018). The impoundment of rivers for hydropower generation, irrigation, flood control or other purposes, changes the landscape and its C cycling (Maavara et al., 2017), often resulting in increased aquatic CO₂ and CH₄ emissions due to the decay of flooded organic matter (Prairie et al., 2018; Venkiteswaran et al., 2013). Globally, reservoirs

30 are estimated to emit between 0.5 and 2.3 PgCO₂eq yr⁻¹ (Barros et al., 2011; Bastviken et al., 2011; Deemer et al., 2016; St. Louis et al., 2000), and this number is predicted to increase with a rapid growth of the hydroelectric sector in the upcoming decades (Zarfl et al., 2015). Several studies have focused on quantifying GHG surface diffusion from reservoirs around the world and have found extremely high variability temporally and spatially (Barros et al., 2011; Deemer et al., 2016), as is found in natural lakes (DelSontro et al., 2018a; Raymond et al., 2013). However, less research exists on the relative contribution of
35 the different sources and processes sustaining surface diffusive fluxes and their variability in reservoirs.

GHG sources to surface waters can be both internal and external. The magnitude of allochthonous inputs, namely terrestrial organic and inorganic C, is known to increase with soil-water connectivity (Hotchkiss et al., 2015), and with soil C content and leaching capacity (Kindler et al., 2011; Li et al., 2017; Monteith et al., 2007). Soil-derived gas inputs are also temporally variable, generally increasing with discharge, like during storm events (Vachon and del Giorgio, 2014) or rainy seasons (Kim
40 et al., 2000; Zhang et al., 2019). Terrestrial inputs in the form of organic C can indirectly sustain surface GHG emissions by fueling lake / reservoir *in situ* organic matter respiration (Karlsson et al., 2007; Pace and Prairie, 2005; Rasilo et al., 2017).

The net internal balance between production and consumption processes of CO₂ and CH₄ influence their surface fluxes. For CO₂, aerobic ecosystem respiration (ER) and gross primary production (GPP) are highly variable in space and time, and generally a function of temperature, organic C content and nutrients (Hanson et al., 2003; Pace and Prairie, 2005; Prairie et al.,
45 1989; Solomon et al., 2013). Net heterotrophy (ER > GPP) is mainly associated with systems receiving high external inputs of organic C (Bogard et al., 2020; Tank et al., 2010; Wilkinson et al., 2016), while net autotrophy (ER < GPP) has been associated with highly productive nutrient-rich systems (Hanson et al., 2003; Sand-Jensen and Staehr, 2009). However, a large part of the variability in measured metabolic rates remains unexplained (Bogard et al., 2020; Coloso et al., 2011; Solomon et al., 2013) impeding our ability to accurately predict their net balance. Additionally, anaerobic C transformation adds another
50 level of complexity to the C metabolic balance by decoupling GPP and ER (Bogard and del Giorgio, 2016; Martinsen et al., 2020; Vachon et al., 2020). For instance, acetoclastic methanogenesis can transform organic C to CH₄ instead of CO₂, and hydrogenotrophic methanogenesis converts CO₂ to CH₄ without producing O₂.

CH₄ is known to be mostly produced in both profundal and littoral sediments, and reach the water surface by vertical or lateral diffusive processes (Bastviken et al., 2008; DelSontro et al., 2018b; Encinas Fernández et al., 2014; Guérin et al., 2016).
55 However, there is increasing evidence that CH₄ production in the oxic water column contributes significantly to lake CH₄ emissions (Bižić et al., 2019; Bogard et al., 2014; DelSontro et al., 2018b; Donis et al., 2017; Tang et al., 2014). Methanogenesis can be counter-balanced by the oxidation of CH₄ to CO₂ mainly in oxic and hypoxic environments (Conrad, 2009; Reis et al., 2020; Thottathil et al., 2019). While several studies have measured rates of CH₄ production and oxidation in lakes and reservoirs, few have quantified the net balance of these two processes at an ecosystem-scale (Bastviken et al., 2008; Schmid et al., 2007; Vachon et al., 2019). According to Vachon et al. (2019), this balance is tightly controlled by physical
60 processes within the water column.

Physical mixing in lakes and reservoirs indirectly impacts C metabolic processes by shaping the O₂ profile, and directly affects GHG surface diffusion by controlling the transport of CO₂ and CH₄ from deep to surface water layers (Barrette and Laprise,

2005; Kreling et al., 2014; Pu et al., 2020). Despite its potential importance (Kankaala et al., 2013), very few studies quantified vertical gas transport and the role of this process in fueling surface GHG emissions. The movement of gases within a system depends on the structure of the water column, which changes spatially along the aquatic continuum. Reservoirs in particular exhibit strong gradients in morphometry and hydrology, translating into high spatial heterogeneity in surface GHG fluxes to the atmosphere (Paranaíba et al., 2018; Teodoru et al., 2011).

Understanding what regulates surface CO₂ and CH₄ concentrations and fluxes to the atmosphere requires knowledge of the interplay between all physical and biogeochemical processes involved, and how they vary spatially. While a number of studies have assessed some processes individually or by difference, very few have measured all relevant components of the epilimnetic mass-balance simultaneously. Here we report on a field study in a tropical East Asian hydropower reservoir quantifying external inputs, sediments inputs, net CO₂ and CH₄ metabolism, vertical diffusion from deeper layers and gas exchange at the air-water interface. This allowed us to estimate the relative contribution of each process in shaping surface GHG emissions from the reservoir, and to test whether the epilimnetic mass balance can be closed. The two major rivers feeding the reservoir flow into two elongated branches, acting as a transition zones, before reaching the main basin. This configuration, common in reservoirs, allowed us to quantify and compare epilimnetic CO₂ and CH₄ regulation in two morphometrically different areas (reservoir branches and main basin). Overall, the aim of this study is to provide an ecosystem-scale portrait of the processes sustaining surface CO₂ and CH₄ emissions and examine how they change when transitioning from a river delta to an open basin.

2 Materials and methods

2.1 Site and sampling description

The study was conducted in Batang Ai hydroelectric reservoir in Sarawak Malaysia (latitude 1.16° and longitude 111.9°). The reservoir is located on the Borneo Island in a tropical equatorial climate with a constantly high temperature averaging 23 °C and 32 °C during nighttime and daytime respectively (Sarawak Government, 2019). The region experiences two weak monsoon seasons (November to February and June to October) with a yearly average rainfall of 3300 to 4600 mm (Sarawak Government, 2019). The reservoir was impounded in 1985 with a dam wall of 85 m, a surface area of ~68.4 km² and a watershed area of 1149 km² of mostly undisturbed forested land (limited rural habitations and small scale croplands).

We distinguish between three sections of the study site: inflows, reservoir branches, and reservoir main basin shown in Fig. 1. The inflows are the two main reservoir inlets: Batang Ai and Engkari rivers (3 to 10 m deep where sampled). The two rivers flow into two arms that we refer to as the reservoir branches (10.8 km², mean and max depths of 18 and 52 m respectively). The reservoir branches merge into the main basin of the reservoir (58.9 km², mean and max depths of 30 and 73 m respectively). Surface sampling was performed in 36 sites across the three study sections, and water column profile sampling (from 0 up to 32 m, each 0.5 to 3 m) was done at 9 sites in the reservoir branches and main basin (Fig. 1). Sampling was repeated (with a

95 few exceptions) during four campaigns: 1) November 14th to December 5th 2016 (Nov-Dec 2016), 2) April 19th to May 3th 2017 (Apr-May 2017), 3) February 28th to March 13th 2018 (Feb-Mar 2018), and 4) August 12th to 29th 2018 (Aug 2018).

2.2 Physical and chemical analyses

Water temperature, dissolved oxygen, and pH were measured using a multi-parameter probe (YSI model 600XLM-M) equipped with a depth gauge and attached to a 12 Volt submersible pump (Proactive Environmental Products model Tornado) for water samples collection. Concentrations of dissolved organic carbon (DOC), total phosphorus (TP), total nitrogen (TN), and chlorophyll a (Chla) were measured during all campaigns in all surface sampling sites (Fig. 1). Methods for these analyses are described in detail in Soued and Prairie (2020). Briefly, TP and Chla (extracted with hot ethanol) were analyzed via spectrophotometry, and TN and DOC (filtered at 0.45 μm) were measured on an Alpkem Flow Solution IV autoanalyser and on a Total Organic Carbon analyser 1010-OI respectively.

105 For each site, we defined the depths of the thermocline and the top and bottom of the metalimnion based on measured temperature profiles using the R package rLakeAnalyzer (Winslow et al., 2018). The epilimnion was defined from the surface to the top of the metalimnion, and was assumed to be a mixed layer.

2.3 Gas concentration, isotopic signature, and water-air fluxes

CO₂ and CH₄ gas concentrations and isotopic signatures ($\delta^{13}\text{C}$) were measured in duplicates at the surface in 36 sites and along vertical profiles in 9 sites (P1 to P9, Fig. 1) using the headspace technique described in details in Soued and Prairie (2020). In brief, sampling was done by equilibrating the water sample for two minutes with an air headspace inside a 60 mL syringe. The gas phase was then injected in a 12 mL pre-vacuumed air-tight vial, and analyzed on a gas chromatograph (Shimadzu GC-8A with a flame ionization detector) for gas concentrations, and on a Cavity Ring Down Spectrometer (CRDS) equipped with a Small Sample Isotopic Module (SSIM, Picarro G2201 -i) for $\delta^{13}\text{C}_{\text{CO}_2}$ and $\delta^{13}\text{C}_{\text{CH}_4}$.

115 Surface gas flux data used in this study are described in more details in Soued and Prairie (2020), a previous study on the C footprint of Batang Ai reservoir. Surface diffusive fluxes of CO₂ and CH₄ were measured at all surface sampling sites during each campaigns. Flux rates were derived from linear changes in CO₂ and CH₄ concentrations in a static floating chamber (design described in Soued and Prairie (2020) and IHA (2010)) connected in a closed loop to a gas analyzer (model UGGA, from Los Gatos Research). Measured gas concentrations, isotopic signature, and fluxes were spatially interpolated to the whole reservoir area by inverse distance weighting (given the absence of a suitable variogram for kriging) using package gstat version 1.1-6 in the R version 3.4.1 software (Pebesma, 2004). Mean values were calculated for each campaign based on the interpolated maps (Soued and Prairie, 2020).

2.4 Horizontal GHG inputs

In order to estimate the external horizontal inputs of CO₂ and CH₄, we considered that the total volume of water inflow and outflow (discharge measured at the dam) were equal, and equivalent to the mean of measured daily discharge (Q, in m³ d⁻¹)

during each campaign (considering minimal changes in inflow / outflow rates during a campaign). The approach of using discharge as a measure of total water inflow has the advantage of integrating all external flow (rivers, lateral soils, and groundwater) as water inputs to the reservoir. However, the fraction of inflow feeding the reservoir surface versus bottom layer, and its average gas concentration can only be approximated based on measurements from the two main river inlets (Fig. 1) due to the lack of data on other lateral inflows. Given that part of the inflowing water is colder and denser than the reservoir surface layer, only a fraction of it enters the epilimnion of the reservoir branches, and the rest plunges into the hypolimnion. We estimated that fraction (f_{epi}) based on temperature profiles in the East river delta and branch (sites P1 and P2, Fig. 1), and assumed it is representative of other water inflows to the reservoir. The areal rate of horizontal CO_2 and CH_4 inputs (H , in $\text{mmol m}^{-2} \text{d}^{-1}$) over each section of the reservoir were then calculated following Eq. (1):

$$H = \frac{C_{in} Q f_{epi}}{A} \quad (1)$$

with A (in m^2) the surface area of the reservoir section considered, and C_{in} (in mmol m^{-3}) the concentration of gas in the inflowing water. To estimate gas inputs from the inflows to the branches, C_{in} was considered as the average of gas concentrations measured at the two upstream extremities of the branches (Fig. 1). To estimate gas inputs from the branches to the main basin, C_{in} was considered as the gas concentrations measured at the confluence between the two branches (right upstream of the main basin).

2.5 Vertical GHG fluxes

We estimated CO_2 and CH_4 fluxes from the metalimnion to the epilimnion (V) based on the vertical gas diffusivity (K_z) and the gradient in gas concentration across the epilimnion-metalimnion interface using Eq. (2) (Wüest and Lorke, 2009):

$$V = K_z (C_{meta} - C_{epi}) \quad (2)$$

where C_{meta} and C_{epi} are the gas concentrations at the top of the metalimnion and at the bottom of the epilimnion respectively, measured in profile sites (P1 to P9, Fig. 1). K_z was derived from the following Eq. (3) (Osborn, 1980):

$$K_z = \Gamma \frac{\epsilon}{N^2} \quad (3)$$

where Γ is the mixing ratio set to 0.2 (Oakey, 1982), ϵ is the dissipation rate of turbulent kinetic energy, and N^2 is the buoyancy frequency. N^2 was calculated from measured temperature profiles (YSI probe) using function `buoyancy.freq` from the `rLakeAnalyzer` package (Winslow et al., 2018) in the R software (R Core Team, 2017). ϵ was derived from measured vertical shear microstructure profiles performed in the Aug 2018 campaign in all profile sites shown in Fig. 1 (except P1 due to floating logs). Shear profiles were measured with a high frequency (512 Hz) MicroCTD profiler (Rockland Scientific) equipped with two velocity shear probes, two thermistors, tilt and vibration sensors, and a pressure sensor. At each site, the profiler was cast 10 times, 5 with an uprising configuration (from bottom to top of the water column) and 5 with a downward configuration (top to bottom), with a 4 min waiting time between profiles to allow water column disturbance to subside. Data quality check and ϵ calculation for each profile cast were performed with ODAS v4.3.03 Matlab library (developed by Rockland Scientific) based on Nasmyth shear spectrum (Oakey, 1982), with ϵ values averaged among the two shear probes and binned over 1-2 m

segments along the profile. For each site, continuous ϵ profiles were interpolated by fitting a smooth spline through all ϵ values from replicate casts as a function of depth.

160 At the epilimnion-metalimnion interface (top of the metalimnion ± 2 m), calculated ϵ averaged 7.7×10^{-9} (range from 3.4×10^{-9} to 1.6×10^{-8}) $\text{m}^2 \text{s}^{-3}$ across all sites sampled with the microCTD, with no significant difference between the main basin and branches sites. In order to estimate vertical gas diffusion, we applied the latter ϵ average to Eq. (2) and (3) for all measured gas profiles (except P1). The resulting V values for each gas were averaged across sites in the main basin and branches separately to derive estimates of V for each of these two reservoir sections.

165 **2.6 Sediment GHG inputs**

We calculated CO_2 and CH_4 inputs from the sediments to epilimnetic waters using gas profiles in sediment cores collected in Apr-May 2017 and Feb-Mar 2018 at 7 sites (P1 to P3 in the reservoir branches and P4, P5, P7, and P9 in the main basin, Fig. 1). Sediment cores were collected using a Glew gravity corer attached to a 6-cm-wide plastic liner. The liner was pre-drilled with 1 cm holes covered with electric tape at each centimeter up to 40 cm. Upon recovery of the sediment core, 3 mL tip-less
170 syringes were inserted into each hole to extract sediments from each centimeter. The sediment content of each syringe was emptied into a 25 mL glass vial prefilled with 6 mL nano-pure water and immediately air-tight sealed by a butyl rubber stopper crimped with an aluminum cap. Glass vials were pressurized with 40 mL of ambient air using a plastic syringe equipped with a needle to pierce the rubber cap. Glass vials were shaken for 2 min for equilibration before extracting the gas with a syringe and injecting it into a pre-evacuated air-tight vial for analysis of CO_2 and CH_4 concentrations and isotopic signatures as
175 described above. Additionally, samples of the water overlaying the sediments (~ 1 cm above) were collected for similar analyses of CO_2 and CH_4 .

Sediment CO_2 and CH_4 flux rates to the overlaying water column were derived from the vertical gradient of gas concentration measured in the sediment cores and overlaying water. The slope of CO_2 or CH_4 concentration as a function of depth (g , in $\mu\text{mol L}^{-1} \text{m}^{-1}$) was calculated for measured values in the first 5 cm of sediments and overlaying water. Most cores exhibited
180 clear linear slopes (p -value < 0.05 and $R^2_{\text{adj}} > 0.5$). In the few cases where a linear slope was not evident, g was replaced by the gradient between the mean gas concentration in the first 3 cm of sediments and the overlaying water. The sediment gas flux rate (S_f in $\text{mmol m}^{-2} \text{d}^{-1}$) were calculated with Eq. (4):

$$S_f = \frac{g \times d}{p} \quad (4)$$

With d the diffusion coefficient set to $1.5 \times 10^{-5} \text{ cm}^2 \text{ s}^{-1}$ (Donis et al., 2017), and p the sediment porosity assumed to be 2 %
185 based on previous results in Batang Ai (Tan, 2015).

At an ecosystem scale, sediment CO_2 and CH_4 inputs to the water column (S) were estimated based on average and standard deviation values of sites located in each section of the reservoir (branches and main basin). For each section, mean sediment CO_2 and CH_4 flux rates were multiplied by the areal ratio of epilimnetic sediments (A_{epi}) versus total water area (A_0). The latter ratio was calculated based on the hypsometric model (Ferland et al., 2014; Imboden, 1973) as shown in Eq. (5) to (7):

$$190 \quad q = \left(\frac{z_{max}}{z_{mean}} \right) - 1 \quad (5)$$

$$A_{epi} = A_0 \left(1 - \left(1 - \left(\frac{z_{epi}}{z_{max}} \right) \right)^q \right) \quad (6)$$

$$S = \frac{A_{epi}}{A_0} S_f \quad (7)$$

with q a parameter describing the general shape of the reservoir section, z_{max} and z_{mean} the maximum and mean depths respectively, and z_{epi} the mean depth of the epilimnion (8.0 and 10.5 m in the branches and main basin respectively).

195 Littoral sediments are known to be a source of CH_4 not only through diffusion but also via ebullition. While this emission pathway was found to be important in other reservoirs (Deemer et al., 2016), it is surprisingly low in Batang Ai, equaling less than 2 % of CH_4 surface diffusive emissions, and only 0.1 % of the reservoir total GHG footprint (Soued and Prairie, 2020). Therefore, sediment ebullition was considered negligible in the epilimnetic CH_4 budget of Batang Ai.

2.7 Metabolic rates

200 Net metabolic rates of CO_2 and CH_4 production in the epilimnetic water column were estimated with *in situ* incubations. Incubations were performed in 5 sites (P2 and P3 in the branches and P4, P5 and P7 in the main basin, Fig. 1). Water from 3 m deep was pumped into 5 L transparent glass jars with an air tight clamp lid. Before closing, jars were filled from the bottom and allowed to overflow, then sampled for initial CO_2 and CH_4 concentrations. Closed jars were fixed at 3 m to an anchored line at the sampling site, and incubated in *in situ* temperature and light conditions for 22.0 to 24.2 hours. Upon retrieval, samples of final CO_2 and CH_4 concentrations were collected from the jars. Volumetric daily rates of net CO_2 and CH_4 production were calculated based on the difference between final and initial gas concentrations rescaled to a 24 h period.

In addition to incubations, open water high frequency O_2 measurements were carried out to derive CO_2 metabolism on larger spatial and temporal scales. Rates of GPP, ER, and net ecosystem production (NEP) were estimated in the reservoir surface layer by monitoring and inverse modeling diel O_2 changes in the epilimnion. O_2 was measured at a one minute interval using high frequency O_2 and temperature sensors (model miniDOT from Precision Measurement Engineering), along with light sensors (model HOBO Pendant from Onset). Sensors were deployed in profile sites P1 to P3 in the branches and P4, P5, P7, and P9 in the main basin (Fig. 1). Note that not all sites were sampled in all sampling campaigns. Sensors were attached to an anchored line at a depth between 0.7 and 3 m and deployment time varied between 4 days and two weeks. Upon retrieval of the sensors, a first data quality check and selection was made based on the sensor internal quality index and visual screening.

215 Rates of ecosystem metabolism were then estimated based on an open system diel O_2 model (Odum, 1956), where change in O_2 concentration is a function of GPP, ER, and air-water gas exchange (K_{O_2}) following Eq. (8) (Hall and Hotchkiss, 2017):

$$\frac{dO_2}{dt} = \frac{GPP}{z_{epi}} + \frac{ER}{z_{epi}} + K_{O_2} (O_{2sat} - O_2) \quad (8)$$

with O_{2sat} the theoretical O_2 concentration at saturation considering the *in situ* temperature and atmospheric pressure, and O_2 is the actual measured O_2 concentration in the water. A detailed description of the model equations can be found in (Hall and

220 Hotchkiss, 2017). Daily estimates of GPP, ER, and K_{600} (based on K_{O_2}) were derived by maximum likelihood fitting of the data to the model in Eq. (8) using the R package StreamMetabolizer (Appling et al., 2018). Note that even though the package used was originally developed for streams, it is easily transferable to lakes given that the model used (Eq. (8)) is generalized for all water bodies, with the parameter z_{epi} describing the depth of a mixed water column of either a lentic or lotic system, and with the K_{600} estimate relying only on data fitting to the model and not on system type. In some cases, where the best predicted
225 K_{600} was negative, the fitting process was rerun with a user defined positive K_{600} , either equal to a value estimated for the previous or subsequent day at the same site (range of 0.03 – 0.96 d^{-1}) or fixed to 0.1 d^{-1} (if no other available estimate). When considering the epilimnion depth, predicted values of K_{600} translate into a 1st to 3rd quantiles range of 1.17 to 5.55 $m d^{-1}$, which is similar to the range of K_{600} values back-calculated from surface gas flux measurements with the floating chamber technique. A final selection of daily metabolic estimates was done based on the model goodness of fit assessed by calculating Pearson
230 correlation coefficient between modeled and measured O_2 values and discarding days with a correlation lower than 0.9. Based on GPP and ER estimates, we calculated daily NEP as the balance between these two processes, and converted it to net CO_2 production rate by assuming an $O_2:CO_2$ metabolic quotient of 1.

Areal metabolic rates were derived by integrating volumetric rates over the depth of the epilimnion. Average estimates of areal metabolic rates per campaign were obtained for the branches and main basin by first averaging data within each site and then
235 across sites for each reservoir section. Note that one value derived from incubations was excluded from the calculation of the average net CH_4 production rate in the branches due to its high value of initial CH_4 concentration (an order of magnitude higher than in all other incubations and all epilimnetic data from this site). The high CH_4 concentration, unrepresentative of real conditions, was probably caused by CH_4 contamination during sampling, and triggered a high oxidation rate that would overestimate the real ecosystem average rate if included.

240 **2.8 Epilimnetic GHG budgets**

Areal rates of horizontal, vertical, sediment, and metabolic inputs were combined into a sum of sources / sinks and compared to the rate of surface gas flux for each gas in each reservoir section. A mean and standard error were calculated for every component of the budgets based on measurements averaged across sites and / or sampling campaigns in order to obtain ecosystem-scale estimates of the components means and uncertainties. In the case of CO_2 metabolism, the ecosystem-scale
245 average was calculated as the mean of the two average values derived from the incubation and diel O_2 monitoring methods. For every component, density curves were derived considering a normal distribution based on the mean and its standard error in order to visualize the relative magnitude and uncertainty of each ecosystem-scale areal rate (Fig. 3).

3 Results

3.1 Physical and chemical properties

250 Surface water temperature exhibited a marked increase from the inflows to the branches, averaging 27.1 and 30.7 °C respectively (Table 1). There was no difference in surface water temperature between the branches and the main basin. The depth of the epilimnion tended to increase and become more stable along the water flow, going from 1.3 (\pm 1.6) m in Batang Ai river delta, to 8.0 (\pm 2.3) m in its branch, and 10.6 (\pm 1.7) m in the main basin (Table 1). Light penetration exhibited the same spatial pattern, with an increasing Secchi depth along the water flow averaging 1.3, 5.1, and 5.5 m in the inflows, 255 branches, and main basin respectively (Table 1). All sections of the study system exhibited oligotrophic water properties (Table 1).

3.2 Surface GHG concentrations, fluxes, and isotopic signatures

Surface CO₂ and CH₄ patterns are summarized in Fig. 2, presenting campaign averages of spatially interpolated gas concentration, flux, and isotopic signature along the different reservoir sections. Despite the temporal variability, the gas 260 patterns along the water flow are robust, remaining similar throughout time (Fig. 2).

Average CO₂ air-water flux and surface concentration were systematically higher in the inflows (mean [range]: 135.3 [18.9 – 368.8] mmol m⁻² d⁻¹ and 58.0 [24.5 – 113.0] μ mol L⁻¹, respectively) compared to the branches (4.7 [-3.4 – 15.2] mmol m⁻² d⁻¹ and 15.4 [12.2 – 19.3] μ mol L⁻¹) and main basin (7.5 [0.3 – 15.1] mmol m⁻² d⁻¹ and 16.0 [14.2 – 17.7] μ mol L⁻¹) (Fig. 2a, b). Surface CO₂ concentration in the reservoir (branches and main basin) was most strongly correlated inversely with water 265 temperature ($R^2_{\text{adj}} = 0.22$, p-value < 0.001, Fig. S1a and Table S1). Except for the Apr-Mar 2017 campaign, there was a modest increase (2.2 to 3.3 ‰) of surface $\delta^{13}\text{CO}_2$ towards more enriched values from the inflows to the branches (Fig. 2c).

Similarly, surface CH₄ flux and concentration continually decreased along the water channel, being an order of magnitude higher in the inflows compared to the branches, and about twice as high in the branches compared to the main basin (Fig. 2d, e). Of all measured water properties, TN was the most strongly linked to reservoir surface CH₄ concentration ($R^2_{\text{adj}} = 0.14$, p-value < 0.001, Fig. S1b and Table S1). In the main basin surface CH₄ concentration significantly decreased with distance to shore in Nov-Dec 2016 ($R^2_{\text{adj}} = 0.54$, p-value < 0.001), but this correlation was weaker ($R^2_{\text{adj}} \leq 0.13$, p-value ≥ 0.03) during other sampling campaigns (Fig. 6a). Surface $\delta^{13}\text{CH}_4$ values varied widely, between -83.3 and -47.6 ‰, but did not show a consistent spatial pattern (Fig. 2f) apart from a positive correlation with distance to shore in the main basin in Nov-Dec 2016 ($R^2_{\text{adj}} = 0.29$, p-value = 0.01, Fig. 6b).

275 The degree of coupling between CO₂ and CH₄ followed a clear spatial pattern. While CO₂ and CH₄ surface concentrations were strongly linked in the inflows ($R^2_{\text{adj}} = 0.54$, p-value = 0.006), they became only weakly correlated in the branches ($R^2_{\text{adj}} = 0.17$, p=0.005) and not correlated at all in the main basin ($R^2_{\text{adj}} = 0.01$, p-value = 0.11) (Fig. S2).

3.3 Horizontal GHG flow

Horizontal inputs from the inflows to the surface layer of the branches were estimated to vary between 0.34 – 0.71 mol s⁻¹ for
280 CO₂ and 0.02 – 0.25 mol s⁻¹ for CH₄. When expressed as rates over the branches surface area (to facilitate comparison with
other components), this results in 2.7 – 5.7 and 0.16 – 1.97 mmol m⁻² d⁻¹ for CO₂ and CH₄ respectively (Table S2 and S3).
These values are in the same order of magnitude as surface fluxes calculated in the branches (Fig. 3a, c, Table S2 and S3).
However, the effect of horizontal inputs faded spatially, with much lower inputs from the branches to the main reservoir basin,
averaging 0.31 and 0.004 mmol m⁻² d⁻¹ for CO₂ and CH₄, respectively (Fig. 3b, d and Table S2 and S3). For CH₄, this fits
285 spatial and temporal surface flux measurements, being systematically higher in the branches, and maximal during the two
sampling campaigns with the highest recorded horizontal inputs from the inflows (Table S3). In contrast, CO₂ surface flux was
typically lower (sometimes negative) in the branches compared to the main basin, despite substantial riverine inputs to the
branches (Table S2).

3.4 Vertical GHG inputs

Vertical fluxes depend on the gas diffusivity and concentration gradient. Gas diffusivity is a function of the strength of
290 stratification (N²) and energy dissipation rate (ε). Measured values of N² and ε varied widely, from 5.9 x 10⁻⁵ to 2.3 x 10⁻³ s⁻²
and from 3.4 x 10⁻⁹ to 1.6 x 10⁻⁸ m² s⁻³ respectively, but with no clear differences between the reservoir branches and main
basin (Fig. S3a, b). Similarly, CO₂ and CH₄ concentration gradients varied substantially in both space and time (from -18.4 to
94.3 μmol L⁻¹ m⁻¹ for CO₂ and -0.19 to 0.4 μmol L⁻¹ m⁻¹ for CH₄). CO₂ concentration generally increased from the epilimnion
295 to the metalimnion as a result of the respiratory CO₂ buildup in the deep layer. On rare occasions, an inverse gradient was
observed, possibly due to autotrophic activity in the metalimnion. For CH₄, metalimnion to epilimnion concentration gradients
were generally modest averaging 0.04 μmol L⁻¹ m⁻¹, and even negative in one third of the profiles leading to the diffusion of
epilimnetic CH₄ toward deeper layers instead of the reverse. The low to negative CH₄ vertical flux results from a highly active
methanotrophic layer reducing CH₄ concentration in the metalimnion, as evidenced by the strong enrichment effect observed
300 in δ¹³CH₄ profiles (Fig. S4). The combination of vertical diffusivity and gas concentration gradients resulted in vertical fluxes
averaging 3.4 (-1.8 to 20.5) mmol m⁻² d⁻¹ for CO₂, and 0.01 (-0.01 to 0.09) mmol m⁻² d⁻¹ for CH₄, with no significant differences
between the reservoir branches and main basin (Fig. S3).

3.5 GHG inputs from littoral sediments

Areal sediment gas fluxes ranged from 1.2 to 4.0 and -0.29 to 1.10 mmol m⁻² d⁻¹ for CO₂ and CH₄, respectively (Fig. S5), in
305 the range of previously reported values in lakes and reservoirs (Adams, 2005; Algesten et al., 2005; Gruca-Rokosz and
Tomaszek, 2015; Huttunen et al., 2006). Sediment fluxes were not different in the branches versus the main basin for both
CO₂ (mean of 2.2 vs 2.4 mmol m⁻² d⁻¹) and CH₄ (mean of 0.17 vs 0.48 mmol m⁻² d⁻¹) (Fig. S5). Applying measured averages
to the area of epilimnetic sediments in each section yields estimates of sediment inputs to the epilimnion of 0.6 (± 0.03) and

0.5 (\pm 0.11) mmol m⁻² d⁻¹ for CO₂, and 0.04 (\pm 0.02) and 0.10 (\pm 0.06) mmol m⁻² d⁻¹ for CH₄ in the branches and main basin
310 respectively (Fig. 3 and Table S2 and S3). These inputs from littoral sediments likely represent an upper limit since they are
based on deep pelagic sediment cores (littoral area were too compact for coring), where a higher organic matter accumulation
and degradation is expected (Blais and Kalff, 1995; Soued and Prairie, 2020). Even as upper estimates, the calculated rates of
sediment GHG inputs remain a relatively modest fraction of the average emissions to the atmosphere for the branches and
main basin both for CO₂ (13 % and 7 %, respectively) and CH₄ (4 % and 23 %, respectively) (Tables S2 and S3).

315 **3.6 Metabolism**

3.6.1 CO₂ metabolism

Estimated GPP and ER rates based on diel O₂ monitoring ranged from 3.6 to 34.5 μ mol L⁻¹ d⁻¹ and from 5.8 to 29.5 μ mol L⁻¹
d⁻¹ respectively (Fig. 4a), which is well within the range of reported rates for oligotrophic systems (Bogard and del Giorgio,
2016; Hanson et al., 2003; Solomon et al., 2013). As expected, GPP and ER rates were correlated ($R^2_{\text{adj}} = 0.23$, p-value <
320 0.001, Fig. 4a), with photosynthesis stimulating the respiration of produced organic matter. In most cases, GPP exceeded ER,
especially in the branches and near aquacultures (Fig. 4a), where higher nutrients (TP and TN) and Chl_a concentrations were
measured (Table 1). Daily metabolic rates showed no correlation with mean daily rain or light (Kendall rank correlation p-
value > 0.1).

In the reservoir branches, results from the diel O₂ monitoring method suggested systematic net CO₂ uptake ranging from -19.2
325 to -1.4 μ mol L⁻¹ d⁻¹, whereas results from two incubations were slightly above that range (-0.5 to 3.3 μ mol L⁻¹ d⁻¹) (Fig. 4b). In
the main basin, incubation results ranged from -8.8 to 7.2 μ mol L⁻¹ d⁻¹, while the diel O₂ technique captured a wider variability
in net CO₂ metabolic rates from -19.2 to 6.1 μ mol L⁻¹ d⁻¹, with an estimated CO₂ uptake in 39 out of 54 cases (Fig. 4b). Areal
net CO₂ metabolic rates, as the average of the two methods, yielded an ecosystem-scale estimate of -23.2 and -11.8 mmol m⁻²
d⁻¹ in the reservoir branches and main basin, respectively (Table S2).

330 To complement the metabolic rate data, surface O₂ and CO₂ departure from saturation were examined in both reservoir sections.
O₂ oversaturation was observed in 44 % of cases in the main basin and 81 % in the branches (Fig. 5), which corresponds with
the spatial patterns of net metabolic rates (Fig. 4b). CO₂ oversaturation was also widespread (74 % of cases), making many
sampled sites oversaturated in both O₂ and CO₂ (55 % in the branches and 32 % in the main basin, Fig. 5).

3.6.2 CH₄ metabolism

335 Net metabolic CH₄ rates (from incubations) ranged from -0.026 to 0.078 μ mol L⁻¹ d⁻¹, indicating that the CH₄ balance in the
epilimnion of Batang Ai varied from net oxidation to net production (Table S3). CH₄ metabolic rates measured in Batang Ai
are within the range of values observed in other systems for oxidation (Guérin and Abril, 2007; Thottathil et al., 2019) and
production (Bogard et al., 2014; Donis et al., 2017). No temporal or spatial (branches versus main basin) differences in net
metabolic CH₄ rate were detected due to a high variability and limited data points.

340 3.7 Ecosystem scale GHG budgets

Estimated sources / sinks of CO₂ and CH₄ were collated into a budget to evaluate their relative impact on epilimnetic gas concentration and to assess whether their sum matches the measured surface gas fluxes in each section of the reservoir. Fig. 3 depicts such reconstruction of the epilimnetic CO₂ and CH₄ budgets in Batang Ai, as well as the uncertainty limits of each component. While each process varied in time, their relative importance in driving surface fluxes was generally similar from
345 one sampling campaign to another (Table S2 and S3).

3.7.1 CO₂ budget

For CO₂, epilimnetic sediment inputs had a small contribution, being typically an order of magnitude lower than measured surface fluxes in both sections of the reservoir (Fig. 3a, b and Table S2). Vertical CO₂ inputs from lower depths on the other hand contributed substantially to surface fluxes in the branches and especially in the main basin (mean of 0.7 and 4.5 mmol
350 m⁻² d⁻¹ respectively, Fig. 3a, b and Table S2), indicating that hypolimnetic processes impact surface emissions despite the permanent stratification. Horizontal inputs of CO₂ averaged 4.3 mmol m⁻² d⁻¹ in the branches, however, they decreased by an order of magnitude when reaching the main basin (mean of 0.3 mmol m⁻² d⁻¹). Thus, direct CO₂ inputs from the inflows notably increase surface flux rates in the reservoir branches but only minimally in the main basin. Net CO₂ metabolism was surprisingly variable (switching from negative to positive NEP on a daily time scale), thus making it difficult to derive a sufficiently precise
355 ecosystem-scale estimate to close the epilimnetic budget (Fig. 3a, b), despite high sampling resolution (n = 66 daily metabolic rates). Including the metabolism substantially shifts the mean of the CO₂ epilimnetic budget (sum of sources and sinks) to a negative value and drastically increases its uncertainty (Fig. 3a, b and Table S2), reflecting a potentially important but poorly resolved role of metabolism in the budget because of its variability. However, given that metabolism acts more likely as a CO₂ sink on average, our best assessment suggests that, vertical transport from deeper layers is the main source sustaining surface
360 CO₂ out-flux in the main basin of Batang Ai.

3.7.2 CH₄ budget

In contrast with CO₂, vertical transport was the smallest source of CH₄ to the epilimnion, contributing to only 2 % of surface fluxes in both reservoir sections (Fig. 3c, d and Table S3). In the branches, sediment inputs and net CH₄ metabolic rates were both relatively low (mean of 0.04 ± 0.02 and 0.04 ± 0.05 mmol m⁻² d⁻¹) and had little impact on the budget, corresponding
365 each to 4 % of surface fluxes in that section (Fig. 3c and Table S3). On the other hand, horizontal inputs were the dominant and most variable source sustaining CH₄ emissions in the branches, where the epilimnetic mass balance closed almost perfectly (Fig. 3c and Table S3). Despite being the main CH₄ source in the branches, horizontal transport was a negligible component in the main basin (1 % of the flux, Fig. 3d and Table S3). Instead, sediment inputs played a larger role in that section, with a mean of 0.10 (± 0.06) mmol m⁻² d⁻¹, fueling 23 % of surface emissions in the main basin (Fig. 3d and Table S3). As with CO₂,
370 the most variable CH₄ component of the mass balance in the main basin was the net metabolism within the epilimnion (mean

of $-0.16 \pm 0.19 \text{ mmol m}^{-2} \text{ d}^{-1}$). Considering all sources, the CH_4 budget indicates a deficit of $0.34 \text{ mmol m}^{-2} \text{ d}^{-1}$ to explain measured surface emissions in the main basin (Fig. 3d and Table S3).

4 Discussion

Our results have highlighted both the importance and the challenges associated with quantifying simultaneously all the components of the epilimnetic CO_2 and CH_4 budgets, particularly in a hydrologically complex reservoir system. While mass fluxes (hydrological, sedimentary, and air-water fluxes) are relatively easy to constrain, internal C processing, namely the net metabolic balances between production and consumption of CO_2 and CH_4 are highly dynamic in both time and space, leading to significant uncertainties when extrapolated to the ecosystem scale. In many studies, some components are only inferred by difference. While convenient from a mass-balance perspective, we argue that assessing all components together is necessary to clearly identify knowledge gaps as well as sources of uncertainty.

4.1 Spatial dynamics of CO_2 and CH_4

The decrease in gas concentration and air-water fluxes along the hydrological continuum observed across sampling campaigns and for both CH_4 and CO_2 reflects a robust spatial structure of the gases. Concurrently, estimates of the horizontal GHG inputs shows a clear and consistent spatial pattern, being high in the branches but negligible in the main basin. A temporal effect of riverine inputs was also observed as the two sampling campaigns with the highest horizontal CH_4 inputs coincided with the highest CH_4 emissions in the branches (Table S3). All these results concord with a progressively reduced influence of direct GHG catchment inputs and greater preponderance of internal processes along the hydrological continuum as observed in river networks (Hotchkiss et al., 2015) and in lakes and reservoirs (Chmiel et al., 2020; Loken et al., 2019; Paranaíba et al., 2018; Pasche et al., 2019).

For CO_2 , the sharpest change in surface metrics (concentration, flux, and isotopic signature) was observed between the inflows and the reservoir branches (Fig. 2a, b, c). Despite large riverine inputs (Table S2), the branches exhibited low CO_2 concentration and fluxes, as well as an increase in $\delta^{13}\text{CO}_2$ matching with high GPP values (Fig. 2a, b, c and 4a). This may reflect increased light availability for phytoplankton when transitioning from the turbid inflows to the reservoir branches (higher Secchi depth, Table 1), a pattern previously reported in other reservoirs (Kimmel and Groeger, 1984; Pacheco et al., 2015; Thornton et al., 1990). While the branch areas are often associated with high CO_2 outflux due to riverine inputs (Beaulieu et al., 2016; Paranaíba et al., 2018; Pasche et al., 2019; Roland et al., 2010; Rudorff et al., 2011), they are occasionally observed to have low air-water flux due to simultaneous nutrient inputs (Loken et al., 2019; Paranaíba et al., 2018; Wilkinson et al., 2016). In Batang Ai, inflows have a high nutrients (TP and TN) to DOC ratio compared to the reservoir branches (Table 1), providing higher inputs of nutrients relative to organic matter, and thus likely stimulating primary production more than respiration. This hypothesis is consistent with a higher GPP: ER ratio and mean Chla concentrations measured in the branches compared to the main basin (Fig. 4a and Table 1). The variability of CO_2 concentration within the reservoir (branches and

main basin) was negatively correlated to temperature, likely due to its effect on GPP (Bogard et al., 2020). This further highlights the important role of primary production in modulating CO₂ dynamics throughout the reservoir, and particularly in the branches.

405 The correlation between surface CH₄ and TN in the reservoir suggests that primary production may also affect CH₄ dynamics. Nutrient content was shown in previous studies to enhance CH₄ production in the sediments (Beaulieu et al., 2019; Gebert et al., 2006; Isidorova et al., 2019) and in the oxic water column (Bogard et al., 2014), through its link with algal production and decomposition. However, CH₄ concentration and flux variability were strongly driven by a spatial / hydrological structure, gradually decreasing from the inflows to the main basin. This likely reflects the combined effect of terrestrial inputs and a
410 decreasing contact of water with sediments along the water channel. Surface δ¹³CH₄ signatures varied substantially but without a consistent spatial pattern (Fig. 2f), indicating that the surface CH₄ pool is shaped by multiple sources / processes (metabolism, riverine, and sediment inputs) varying through space and time.

The changing relative contribution of sources and processes shaping surface CO₂ and CH₄ concentrations varies with the system hydro-morphology, from the inflows to the main reservoir basin, and lead to a progressive decoupling between the two
415 gases along the continuum (Fig. S2). The observed CO₂ and CH₄ coupling in the inflows and branches is associated to a common catchment source, as previously reported in other systems including soil-water (Lupon et al., 2019), streams (Rasilo et al., 2017), and lake and reservoir inflow areas (Loken et al., 2019; Natchimuthu et al., 2017; Paranaíba et al., 2018). Indeed, horizontal inputs are the main source of both CO₂ and CH₄ in the upstream reaches of Batang Ai, accounting on average for 91 and 92 % of their respective surface out-flux in the branch section (Fig. 3a, c and Tables S2 and S3). However, when
420 reaching the main basin, driving sources diverge between the two gases, with vertical inputs from the bottom layer supporting on average 60 % of CO₂ compared to 2 % of CH₄ fluxes, while sediment inputs sustained 7 versus 23 % of CO₂ and CH₄ fluxes respectively in that section. This decoupling partly results from the two gases having distinct metabolic pathways: mainly aerobic for CO₂ and anaerobic for CH₄, leading to their sources and sinks being spatially disconnected in the main basin. Consequently, sediments being a mostly anaerobic environment are a more important source of CH₄ relative to CO₂, while the
425 metalimnetic layer being oxic-hypoxic acts as a sink of CH₄ and source of CO₂ via aerobic CH₄ oxidation (Fig. S4). Overall, the spatial patterns reported here highlight the hydrodynamic zonation common in reservoirs and its diverging effect on CO₂ versus CH₄ cycling.

4.2 CO₂ metabolism

Our observation that GPP often exceeded ER (Fig. 4a) was not unexpected given the very low DOC concentration (< 1 mg L⁻¹).
430 Previous work has reported that DOC > 4 mg L⁻¹ is required to sustain persistent net heterotrophy and CO₂ evasion (Hanson et al., 2003; Prairie et al., 2002). Throughout the reservoir, we found high day-to-day variability in both ER and GPP, but with no apparent link to weather data (light and rain, data not shown). The absence of such a link at a daily time scale has been previously reported (Coloso et al., 2011), while other studies associated daily variations in metabolism with changes in water inflows carrying nutrients (Pacheco et al., 2015; Staehr and Sand-Jensen, 2007), or thermocline stability regulating

435 hypolimnetic water incursions to the epilimnion. Such variations in thermocline depth are thought to be more common in warm tropical systems (Lewis, 2010), and were observed across sampling campaigns in Batang Ai, especially in the branches where the depth of the mixed layer varied considerably ($SD = 2.3$ m, Table 1). Hence, hydrological and physical factors may regulate spatial and daily patterns of GPP and ER rates in Batang Ai through their influence on nutrient dynamics.

The accuracy of rates derived from diel O_2 monitoring partly depends on the respiratory and photosynthetic quotients (RQ and
440 PQ) assumed for the conversion of metabolic rates from O_2 to CO_2 . A quotient differing from the assumed 1:1 ratio can lead to an under or over-estimation of net CO_2 production. The fact that net CO_2 metabolic rates were on average higher in incubations, based on direct CO_2 measurements compared to diel O_2 monitoring (Fig. 4b and Table S2), hints at a deviation of the metabolic quotients from unity in Batang Ai. Additionally, surface O_2 versus CO_2 concentrations shows that the departure of these gases from saturation varies widely around the expected 1:-1 line, with many surface samples oversaturated
445 in both O_2 and CO_2 , especially in the branches (Fig. 5). This indicates an excess O_2 and / or CO_2 that can be due to a PQ and / or a RQ higher than 1, or to external CO_2 inputs to the epilimnion (Vachon et al., 2020), for instance from the inflows or the bottom layer (Table S2). Metabolic quotients have been shown to vary widely, depending on the type and magnitude of photochemical and biological reactions at play (Berggren et al., 2012; Lefèvre and Merlivat, 2012; Vachon et al., 2020; Williams and Robertson, 1991). For instance, CH_4 oxidation and production, evidently occurring in Batang Ai's epilimnion
450 (Table S2 and S3), diverge from the metabolic $O_2:CO_2$ ratio of one, with CH_4 oxidation consuming two moles of O_2 for each mole of CO_2 produced, and acetoclastic methanogenesis producing CO_2 without O_2 consumption. Even though net CH_4 processing rates are a minor portion of the epilimnetic C cycling in Batang Ai (1-2 orders of magnitudes lower than CO_2 metabolic rates, Tables S2 and S3), these reactions (and other unmeasured processes) have the potential to alter the $O_2:CO_2$ metabolic quotient at an ecosystem scale. The lack of direct measure of metabolic quotients in Batang Ai adds uncertainty to
455 the net CO_2 metabolism estimates based on O_2 data. The observed decoupling of O_2 and CO_2 metabolism in Batang Ai highlights the need for a deeper understanding of the biochemical reactions occurring in the epilimnion, and their effect on metabolic quotients.

Overall, our results from Batang Ai reservoir point to water column metabolism as both a key process in the CO_2 epilimnetic budget and a challenging one to estimate at an ecosystem scale (Fig. 3a, b). Improving this requires a better mechanistic
460 knowledge of the physical and biochemical processes at play and how they interact to shape NEP.

4.3 CH_4 metabolism

Incubation results exhibited a wide range of net CH_4 metabolism: from net oxidation to net production. CH_4 oxidation is known to be highly dependent on CH_4 availability and is optimal in low oxygen and low light conditions (Borrel et al., 2011; Thottathil et al., 2018, 2019), whereas CH_4 production in the oxic water is still poorly understood but have been frequently linked to
465 phytoplankton growth (Berg et al., 2014; Bogard et al., 2014; Lenhart et al., 2015; Wang et al., 2017). A large variability in results exists among the studies that have assessed the net balance of CH_4 metabolism in the water column, with some studies reporting pelagic CH_4 production as a largely dominant process (Donis et al., 2017) while others find no trace of it (Bastviken

et al., 2008). Based on spatial patterns of surface CH₄ concentration and isotopic signature with distance to shore, DelSontro et al. (2018b) showed that, in 30 % of their studied temperate lakes, CH₄ oxidation was dominant versus 70 % dominated by net pelagic production. In Batang Ai, surface δ¹³CH₄ values were highly variable (-82.5 to -47.7 ‰) but mostly uncorrelated with distance to shore, except a positive correlation indicative of oxidation in the Nov-Dec 2016 (R²_{adj} = 0.29, p-value = 0.01, Fig. 6b) coinciding with a strong inverse pattern for CH₄ concentration (R²_{adj} = 0.54, p-value < 0.001, Fig. 6a). This suggests a temporal shift in processes driving surface CH₄ patterns. Also, some measured surface δ¹³CH₄ values were lower than the mean δ¹³CH₄ from the sediments (-66.0 ‰, unpublished data), suggesting another highly depleted source of pelagic CH₄ in the system. This is in line with water incubation results often showing positive net CH₄ production (Table S3). When reported as mean areal rates, CH₄ metabolism ranged from net consumption to net production of CH₄ (-0.29 to 0.94 mmol.m⁻².d⁻¹), which reflects its potential in having a high impact, either positive or negative, on the epilimnetic CH₄ budget at the reservoir scale (Fig. 3d and Table S3). Results in Batang Ai show that the net balance of CH₄ metabolic processes varies widely even within a single system. However, the factors regulating this balance remain largely unknown. Investigating such factors constitute a key step in resolving CH₄ budgets in lakes and reservoirs.

4.4 Epilimnetic GHG budgets

For CO₂, measured surface fluxes in both reservoir sections fall in the range of possible values estimated by the sum of epilimnetic processes and their uncertainties (Fig. 3a, b and Table S2). However, the averages of those two terms differ substantially, due to negative values of metabolism shifting the mean of the mass balance towards net CO₂ consumption whereas, on average, surface out-flux was measured from the reservoir. This discrepancy indicates either a missing source of CO₂ in the budget or the underestimation of one of the processes. While lateral groundwater input is a potential source not explicitly considered, it is probably modest given the small ratio of littoral area to epilimnion volume, and is unlikely to account for the large CO₂ deficit in the budget. On the other hand, underestimation of the CO₂ metabolic balance is much more likely, given its large variability and uncertainty around its mean value. Additionally, a systematic underestimation of the CO₂ metabolic rates derived from the diel O₂ method is very possible in Batang Ai given the likely deviation of metabolic quotients around the 1:1 line. As an example, when setting the photosynthetic quotient to 1.2 instead of 1, which remains well within the literature range (Lefèvre and Merlivat, 2012; Williams and Robertson, 1991), the average epilimnetic CO₂ mass balance would increase from -17.7 to 4.3 mmol m⁻² d⁻¹ in the branches and from -6.5 to 6.2 mmol m⁻² d⁻¹ in the main basin, closely matching measured surface fluxes of 4.7 and 7.5 mmol m⁻² d⁻¹ in the respective sections. Thus, constraining the metabolic component, especially the O₂: CO₂ quotients, is key for closing the CO₂ epilimnetic budget.

In the case of CH₄, the epilimnetic mass balance in the branches is surprisingly close to the observed surface flux, largely fueled by horizontal inputs. Hence, CH₄ emissions from the branches reflect catchment CH₄ loads rather than internal processes. However, in the main basin, these inputs become negligible and the estimated budget does not match measured emissions, indicating a deficit of 0.49 mmolCH₄ m⁻² d⁻¹. This amount cannot be explained by a potential underestimation of horizontal or vertical inputs since they are two orders of magnitude lower. Similarly, sediment inputs would need to be six

time higher than estimated to fulfill the budget deficit, which is unlikely given their much lower range of uncertainty. Thus, the most plausible source to close the mass balance in the main basin would be water column CH₄ production. Although the estimated CH₄ metabolism indicates an average net consumption rather than a net production (-0.16 mmol m⁻² d⁻¹), this mean value is based on only 3 data points and has a high uncertainty associated to it (SE = 0.19 mmol m⁻² d⁻¹, Table S3). Closing the mass balance would require a net volumetric CH₄ production of about 0.03 μmol L⁻¹ d⁻¹ in the water column of the main basin. This value seems plausible since an equal production rate was measured in one of the incubations, and it is at the low end of the range reported in other systems (Bogard *et al.*, 2014 ; DelSontro *et al.*, 2018b ; Donis *et al.*, 2017). The combination of our results suggests that water column metabolism could be the dominant source of CH₄ in the main basin of Batang Ai, potentially sustaining up to 75 % of surface emissions in that reservoir section. However, this process seems highly dynamic and requires more intensive research into its controls at spatial and temporal scales, commensurate with CH₄ emissions.

5 Conclusion

The estimated epilimnetic CO₂ and CH₄ budgets in Batang Ai has helped define the role of different processes in shaping the reservoir surface GHG fluxes to the atmosphere. Results showed that horizontal riverine inputs are important sources of GHG in the reservoir branches (especially for CH₄). This creates a coupling between CO₂ and CH₄ close to the river deltas, which gradually fades along the water flow, until the surface concentrations of the two gases become completely uncoupled in the main basin being driven by different sources. For instance, vertical inputs from the bottom layer contributed significantly to surface CO₂ saturation, while being negligible in the case of CH₄ due to metalimnetic oxidation. Inversely, sediment inputs played a notably greater role in sustaining epilimnetic oversaturation of CH₄ compared to CO₂ in the main basin. Nonetheless, the epilimnetic budgets of both gases presented a high sensitivity to water column metabolism. This result is likely representative of large systems with a high volume of water versus sediments, which is common for hydroelectric reservoirs. However, metabolic balances of CO₂ and CH₄ were extremely variable in space and time, switching from a net production to a net consumption of the gases, and leading to highly uncertain ecosystem-scale estimates, which emphasizes the key but unconstrained role of metabolism in the overall GHG budgets. Factors driving these metabolic changes are not well defined based on current knowledge, highlighting the need for further research on the subject. Overall, this study gives an integrative portrait of the relative contribution of different sources to surface CO₂ and CH₄ fluxes in a permanently stratified reservoir including its transition zones (branches). Conclusions and insights derived from this work likely reflect C dynamics in other similar systems, and highlight knowledge gaps guiding future research to better understand and predict aquatic GHG fluxes and regulation.

Author contribution

- 530 CS contributed to conceptualization, methodology, validation, formal analysis, investigation, data curation, writing - original draft, writing – review and editing, and project administration. YTP contributed to Methodology, validation, investigation, resources, writing – review and editing, supervision, and funding acquisition.

Competing interests

The authors declare that they have no conflict of interest.

535 Acknowledgments

- This work was funded by Sarawak Energy Berhad and the Natural Science and Engineering Research Council of Canada (Discovery grant to Y.T.P. and BES-D scholarship to C.S.). We are grateful to Karen Lee Suan Ping and Jenny Choo Cheng Yi for their logistic support and participation in sampling campaigns. We also thank Jessica Fong Fung Yee, Amar Ma'aruf Bin Ismawi, Gerald Tawie Anak Thomas, Hilton Bin John, Paula Reis, Sara Mercier-Blais and Karelle Desrosiers for their
540 help on the field, and Katherine Velghe and Marilyne Robidoux for their assistance during laboratory analyses.

References

- Adams, D. D.: Diffuse Flux of Greenhouse Gases — Methane and Carbon Dioxide — at the Sediment-Water Interface of Some Lakes and Reservoirs of the World, in *Greenhouse Gas Emissions - Fluxes and Processes*, pp. 129–153., 2005.
- 545 Algesten, G., Sobek, S., Bergström, A. K., Jonsson, A., Tranvik, L. J. and Jansson, M.: Contribution of sediment respiration to summer CO₂ emission from low productive boreal and subarctic lakes, *Microb. Ecol.*, 50(4), 529–535, doi:10.1007/s00248-005-5007-x, 2005.
- Appling, A. P., Hall, R. O., Arroita, M. and Yackulic, C. B.: StreamMetabolizer: Models for Estimating Aquatic Photosynthesis and Respiration, [online] Available from: <https://github.com/USGS-R/streamMetabolizer>, 2018.
- 550 Barrette, N. and Laprise, R.: A One-Dimensional Model for Simulating the Vertical Transport of Dissolved CO₂ and CH₄ in Hydroelectric Reservoirs, in *Greenhouse Gas Emissions - Fluxes and Processes*, pp. 575–595., 2005.
- Barros, N., Cole, J. J., Tranvik, L. J., Prairie, Y. T., Bastviken, D., Huszar, V. L. M., del Giorgio, P. and Roland, F.: Carbon emission from hydroelectric reservoirs linked to reservoir age and latitude, *Nat. Geosci.*, 4(9), 593–596, doi:10.1038/ngeo1211, 2011.

- 555 Bastviken, D., Cole, J. J., Pace, M. L. and Van de-Bogert, M. C.: Fates of methane from different lake habitats: Connecting whole-lake budgets and CH₄ emissions, *J. Geophys. Res. Biogeosciences*, 113(2), 1–13, doi:10.1029/2007JG000608, 2008.
- Bastviken, D., Tranvik, L. J., Downing, J. A., Crill, P. M. and Enrich-Prast, A.: Freshwater Methane Emissions Offset the Continental Carbon Sink, *Science* (80-.), 331(6013), 50–50, doi:10.1126/science.1196808, 2011.
- 560 Beaulieu, J. J., McManus, M. G. and Nietch, C. T.: Estimates of reservoir methane emissions based on a spatially balanced probabilistic-survey, *Limnol. Oceanogr.*, 61(S1), S27–S40, doi:10.1002/lno.10284, 2016.
- Beaulieu, J. J., DelSontro, T. and Downing, J. A.: Eutrophication will increase methane emissions from lakes and impoundments during the 21st century, *Nat. Commun.*, 10(1), 3–7, doi:10.1038/s41467-019-09100-5, 2019.
- Berg, A., Lindblad, P. and Svensson, B. H.: Cyanobacteria as a source of hydrogen for methane formation, *World J. Microbiol. Biotechnol.*, 30(2), 539–545, doi:10.1007/s11274-013-1463-5, 2014.
- 565 Berggren, M., Lapierre, J.-F. and del Giorgio, P. A.: Magnitude and regulation of bacterioplankton respiratory quotient across freshwater environmental gradients, *ISME J.*, 6(5), 984–993, doi:10.1038/ismej.2011.157, 2012.
- Bižić, M., Klintzsch, T., Ionescu, D., Hindyieh, M., Guentzel, M., Muro-Pastor, A. M., Eckert, W., Urich, T., Keppler, F. and Grossart, H.-P.: Aquatic and terrestrial Cyanobacteria produce methane, *Sci. Adv.*, (13), In Press, 2019.
- 570 Blais, J. M. and Kalff, J.: The influence of lake morphometry on sediment focusing, *Limnol. Oceanogr.*, 40(3), 582–588, doi:10.4319/lno.1995.40.3.0582, 1995.
- Bogard, M. J. and del Giorgio, P. A.: The role of metabolism in modulating CO₂ fluxes in boreal lakes, *Global Biogeochem. Cycles*, 30(10), 1509–1525, doi:10.1002/2016GB005463, 2016.
- Bogard, M. J., del Giorgio, P. a, Boutet, L., Chaves, M. C. G., Prairie, Y. T., Merante, A. and Derry, A. M.: Oxidic water column methanogenesis as a major component of aquatic CH₄ fluxes., *Nat. Commun.*, 5(May), 5350, doi:10.1038/ncomms6350, 2014.
- 575 Bogard, M. J., St-Gelais, N. F., Vachon, D. and del Giorgio, P. A.: Patterns of Spring/Summer Open-Water Metabolism Across Boreal Lakes, *Ecosystems*, doi:10.1007/s10021-020-00487-7, 2020.
- Borrel, G., Jézéquel, D., Biderre-Petit, C., Morel-Desrosiers, N., Morel, J. P., Peyret, P., Fonty, G. and Lehours, A. C.: Production and consumption of methane in freshwater lake ecosystems, *Res. Microbiol.*, 162(9), 832–847, doi:10.1016/j.resmic.2011.06.004, 2011.

- 580 Chmiel, H. E., Hofmann, H., Sobek, S., Efremova, T. and Pasche, N.: Where does the river end? Drivers of spatiotemporal variability in CO₂ concentration and flux in the inflow area of a large boreal lake, *Limnol. Oceanogr.*, 65(6), 1161–1174, doi:10.1002/lno.11378, 2020.
- Coloso, J. J., Cole, J. J. and Pace, M. L.: Difficulty in Discerning Drivers of Lake Ecosystem Metabolism with High-Frequency Data, *Ecosystems*, 14(6), 935–948, doi:10.1007/s10021-011-9455-5, 2011.
- 585 Conrad, R.: The global methane cycle: recent advances in understanding the microbial processes involved, *Environ. Microbiol. Rep.*, 1(5), 285–292, doi:10.1111/j.1758-2229.2009.00038.x, 2009.
- Deemer, B. R., Harrison, J. A., Li, S., Beaulieu, J. J., DelSontro, T., Barros, N., Bezerra-Neto, J. F., Powers, S. M., dos Santos, M. A. and Vonk, J. A.: Greenhouse Gas Emissions from Reservoir Water Surfaces: A New Global Synthesis, *Bioscience*, 66(11), 949–964, doi:10.1093/biosci/biw117, 2016.
- 590 DelSontro, T., Beaulieu, J. J. and Downing, J. A.: Greenhouse gas emissions from lakes and impoundments: Upscaling in the face of global change, *Limnol. Oceanogr. Lett.*, 3(3), 64–75, doi:10.1002/lol2.10073, 2018a.
- DelSontro, T., del Giorgio, P. A. and Prairie, Y. T.: No Longer a Paradox: The Interaction Between Physical Transport and Biological Processes Explains the Spatial Distribution of Surface Water Methane Within and Across Lakes, *Ecosystems*, 21(6), 1073–1087, doi:10.1007/s10021-017-0205-1, 2018b.
- 595 Donis, D., Flury, S., Stöckli, A., Spangenberg, J. E., Vachon, D. and McGinnis, D. F.: Full-scale evaluation of methane production under oxic conditions in a mesotrophic lake, *Nat. Commun.*, 8(1), 1–11, doi:10.1038/s41467-017-01648-4, 2017.
- Encinas Fernández, J., Peeters, F. and Hofmann, H.: Importance of the autumn overturn and anoxic conditions in the hypolimnion for the annual methane emissions from a temperate lake, *Environ. Sci. Technol.*, 48(13), 7297–7304, doi:10.1021/es4056164, 2014.
- 600 Ferland, M. E., Prairie, Y. T., Teodoru, C. and Del Giorgio, P. A.: Linking organic carbon sedimentation, burial efficiency, and long-term accumulation in boreal lakes, *J. Geophys. Res. Biogeosciences*, 119(5), 836–847, doi:10.1002/2013JG002345, 2014.
- Gebert, J., Köthe, H. and Gröngröft, A.: Prognosis of methane formation by river sediments, *J. Soils Sediments*, 6(2), 75–83, doi:10.1065/jss2006.04.153, 2006.
- 605 Gruca-Rokosz, R. and Tomaszek, J. A.: Methane and carbon dioxide in the sediment of a eutrophic reservoir: Production pathways and diffusion fluxes at the sediment-water interface, *Water. Air. Soil Pollut.*, 226(2), doi:10.1007/s11270-014-2268-3, 2015.

- Guérin, F. and Abril, G.: Significance of pelagic aerobic methane oxidation in the methane and carbon budget of a tropical reservoir, *J. Geophys. Res. Biogeosciences*, 112(G3), n/a–n/a, doi:10.1029/2006JG000393, 2007.
- 610 Guérin, F., Deshmukh, C., Labat, D., Pighini, S., Vongkhamsoo, A., Guédant, P., Rode, W., Godon, A., Chanudet, V., Descloux, S. and Serça, D.: Effect of sporadic destratification, seasonal overturn, and artificial mixing on CH₄ emissions from a subtropical hydroelectric reservoir, *Biogeosciences*, 13(12), 3647–3663, doi:10.5194/bg-13-3647-2016, 2016.
- Hall, R. O. and Hotchkiss, E. R.: Stream Metabolism, in *Methods in Stream Ecology*, vol. 2, pp. 219–233, Elsevier., 2017.
- Hanson, P. C., Bade, D. L., Carpenter, S. R. and Kratz, T. K.: Lake metabolism: Relationships with dissolved organic carbon and phosphorus, *Limnol. Oceanogr.*, 48(3), 1112–1119, doi:10.4319/lo.2003.48.3.1112, 2003.
- 615 Hotchkiss, E. R., Hall Jr, R. O., Sponseller, R. A., Butman, D., Klaminder, J., Laudon, H., Rosvall, M. and Karlsson, J.: Sources of and processes controlling CO₂ emissions change with the size of streams and rivers, *Nat. Geosci.*, 8(9), 696–699, doi:10.1038/ngeo2507, 2015.
- Huttunen, J. T., Väisänen, T. S., Hellsten, S. K. and Martikainen, P. J.: Methane fluxes at the sediment-water interface in some boreal lakes and reservoirs, *Boreal Environ. Res.*, 11(1), 27–34, 2006.
- 620 Imboden, D. M.: Limnologische Transport- und Nährstoffmodelle, *Schweizerische Zeitschrift für Hydrol.*, 35(1), 29–68, doi:10.1007/BF02502063, 1973.
- International Hydropower Association (IHA): GHG measurement guidelines for freshwater reservoirs., 2010.
- Isidorova, A., Grasset, C., Mendonça, R. and Sobek, S.: Methane formation in tropical reservoirs predicted from sediment age and nitrogen, *Sci. Rep.*, 9(1), 1–9, doi:10.1038/s41598-019-47346-7, 2019.
- 625 Kankaala, P., Huotari, J., Tulonen, T. and Ojala, A.: Lake-size dependent physical forcing drives carbon dioxide and methane effluxes from lakes in a boreal landscape, *Limnol. Oceanogr.*, 58(6), 1915–1930, doi:10.4319/lo.2013.58.6.1915, 2013.
- Karlsson, J., Jansson, M. and Jonsson, A.: Respiration of allochthonous organic carbon in unproductive forest lakes determined by the Keeling plot method, *Limnol. Oceanogr.*, 52(2), 603–608, doi:10.4319/lo.2007.52.2.0603, 2007.
- 630 Kim, B., Choi, K., Kim, C., Lee, U. H. and Kim, Y. H.: Effects of the summer monsoon on the distribution and loading of organic carbon in a deep reservoir, Lake Soyang, Korea, *Water Res.*, 34(14), 3495–3504, doi:10.1016/S0043-1354(00)00104-4, 2000.

- Kimmel, B. L. and Groeger, A. W.: Factors Controlling Primary Production in Lakes and Reservoirs: a Perspective, *Lake Reserv. Manag.*, 1(1), 277–281, doi:10.1080/07438148409354524, 1984.
- 635 Kindler, R., Siemens, J., Kaiser, K., Walmsley, D. C., Bernhofer, C., Buchmann, N., Cellier, P., Eugster, W., Gleixner, G., Grunwald, T., Heim, A., Ibrom, A., Jones, S. K., Jones, M., Klumpp, K., Kutsch, W., Larsen, K. S., Lehuger, S., Loubet, B., Mckenzie, R., Moors, E., Osborne, B., Pilegaard, K., Rebmann, C., Saunders, M., Schmidt, M. W. I., Schrumpp, M., Seyfferth, J., Skiba, U., Soussana, J. F., Sutton, M. A., Tefs, C., Vowinckel, B., Zeeman, M. J. and Kaupenjohann, M.: Dissolved carbon leaching from soil is a crucial component of the net ecosystem carbon balance, *Glob. Chang. Biol.*, 17(2), 1167–1185, doi:10.1111/j.1365-2486.2010.02282.x, 2011.
- 640 Kreling, J., Bravidor, J., McGinnis, D. F., Koschorreck, M. and Lorke, A.: Physical controls of oxygen fluxes at pelagic and benthic oxyclines in a lake, *Limnol. Oceanogr.*, 59(5), 1637–1650, doi:10.4319/lo.2014.59.5.1637, 2014.
- Lefèvre, N. and Merlivat, L.: Carbon and oxygen net community production in the eastern tropical Atlantic estimated from a moored buoy, *Global Biogeochem. Cycles*, 26(1), n/a–n/a, doi:10.1029/2010GB004018, 2012.
- 645 Lenhart, K., Klintzsch, T., Langer, G., Nehrke, G., Bunge, M., Schnell, S. and Keppler, F.: Evidence for methane production by marine algae (*Emiliana huxleyi*) and its implication for the methane paradox in oxic waters, *Biogeosciences Discuss.*, 12(24), 20323–20360, doi:10.5194/bgd-12-20323-2015, 2015.
- Lewis, W. M.: Biogeochemistry of tropical lakes, *SIL Proceedings*, 1922-2010, 30(10), 1595–1603, doi:10.1080/03680770.2009.11902383, 2010.
- 650 Li, M., Peng, C., Wang, M., Xue, W., Zhang, K., Wang, K., Shi, G. and Zhu, Q.: The carbon flux of global rivers: A re-evaluation of amount and spatial patterns, *Ecol. Indic.*, 80(April), 40–51, doi:10.1016/j.ecolind.2017.04.049, 2017.
- Loken, L. C., Crawford, J. T., Schramm, P. J., Stadler, P., Desai, A. R. and Stanley, E. H.: Large Spatial and Temporal Variability of Carbon Dioxide and Methane in a Eutrophic Lake, *J. Geophys. Res. Biogeosciences*, 124(7), 2248–2266, doi:10.1029/2019JG005186, 2019.
- 655 St. Louis, V. L., Kelly, C. A., Duchemin, É., Rudd, J. W. M. and Rosenberg, D. M.: Reservoir Surfaces as Sources of Greenhouse Gases to the Atmosphere: A Global Estimate, *Bioscience*, 50(9), 766–775, doi:10.1641/0006-3568(2000)050[0766:RSASOG]2.0.CO;2, 2000.
- Lupon, A., Denfeld, B. A., Laudon, H., Leach, J., Karlsson, J. and Sponseller, R. A.: Groundwater inflows control patterns and sources of greenhouse gas emissions from streams, *Limnol. Oceanogr.*, 64(4), 1545–1557, doi:10.1002/lno.11134, 2019.
- 660 Maavara, T., Lauerwald, R., Regnier, P. and Van Cappellen, P.: Global perturbation of organic carbon cycling by river damming, *Nat. Commun.*, 8(May), 1–10, doi:10.1038/ncomms15347, 2017.

- Martinsen, K. T., Kragh, T. and Sand-Jensen, K.: Carbon dioxide efflux and ecosystem metabolism of small forest lakes, *Aquat. Sci.*, 82(1), 9, doi:10.1007/s00027-019-0682-8, 2020.
- 665 Monteith, D. T., Stoddard, J. L., Evans, C. D., De Wit, H. A., Forsius, M., Høgåsen, T., Wilander, A., Skjelkvåle, B. L., Jeffries, D. S., Vuorenmaa, J., Keller, B., Kopécek, J. and Vesely, J.: Dissolved organic carbon trends resulting from changes in atmospheric deposition chemistry, *Nature*, 450(7169), 537–540, doi:10.1038/nature06316, 2007.
- Natchimuthu, S., Sundgren, I., Gålfalk, M., Klemetsson, L. and Bastviken, D.: Spatiotemporal variability of lake pCO₂ and CO₂ fluxes in a hemiboreal catchment, *J. Geophys. Res. Biogeosciences*, 122(1), 30–49, doi:10.1002/2016JG003449, 2017.
- 670 Oakey, N. S.: Determination of the Rate of Dissipation of Turbulent Energy from Simultaneous Temperature and Velocity Shear Microstructure Measurements, *J. Phys. Oceanogr.*, 12(3), 256–271, doi:10.1175/1520-0485(1982)012<0256:DOTROD>2.0.CO;2, 1982, 1982.
- Odum, H. T.: Primary Production in Flowing Waters¹, *Limnol. Oceanogr.*, 1(2), 102–117, doi:10.4319/lo.1956.1.2.0102, 1956.
- 675 Osborn, T. R.: Estimates of the Local Rate of Vertical Diffusion from Dissipation Measurements, *J. Phys. Oceanogr.*, 10(1), 83–89, doi:10.1175/1520-0485(1980)010<0083:EOTLRO>2.0.CO;2, 1980.
- Pace, M. L. and Prairie, Y. T.: Respiration in lakes, in *Respiration in Aquatic Ecosystems*, pp. 103–121, Oxford University Press., 2005.
- 680 Pacheco, F. S., Soares, M. C. S., Assireu, A. T., Curtarelli, M. P., Roland, F., Abril, G., Stech, J. L., Alvalá, P. C. and Ometto, J. P.: The effects of river inflow and retention time on the spatial heterogeneity of chlorophyll and water–air CO₂ fluxes in a tropical hydropower reservoir, *Biogeosciences*, 12(1), 147–162, doi:10.5194/bg-12-147-2015, 2015.
- Paranaíba, J. R., Barros, N., Mendonça, R., Linkhorst, A., Isidorova, A., Roland, F., Almeida, R. M. and Sobek, S.: Spatially Resolved Measurements of CO₂ and CH₄ Concentration and Gas-Exchange Velocity Highly Influence Carbon-Emission Estimates of Reservoirs, *Environ. Sci. Technol.*, 52(2), 607–615, doi:10.1021/acs.est.7b05138, 2018.
- 685 Pasche, N., Hofmann, H., Bouffard, D., Schubert, C. J., Lozovik, P. A. and Sobek, S.: Implications of river intrusion and convective mixing on the spatial and temporal variability of under-ice CO₂, *Inl. Waters*, 2041, doi:10.1080/20442041.2019.1568073, 2019.
- Pebesma, E. J.: Multivariable geostatistics in S: the gstat package, *Comput. Geosci.*, 30(7), 683–691, doi:10.1016/j.cageo.2004.03.012, 2004.

- 690 Prairie, Y. T., Duarte, C. M. and Kalff, J.: Unifying Nutrient–Chlorophyll Relationships in Lakes, *Can. J. Fish. Aquat. Sci.*, 46(7), 1176–1182, doi:10.1139/f89-153, 1989.
- Prairie, Y. T., Bird, D. F. and Cole, J. J.: The summer metabolic balance in the epilimnion of southeastern Quebec lakes, *Limnol. Oceanogr.*, 47(1), 316–321, doi:10.4319/lo.2002.47.1.0316, 2002.
- 695 Prairie, Y. T., Alm, J., Beaulieu, J., Barros, N., Battin, T., Cole, J., del Giorgio, P., DelSontro, T., Guérin, F., Harby, A., Harrison, J., Mercier-Blais, S., Serça, D., Sobek, S. and Vachon, D.: Greenhouse Gas Emissions from Freshwater Reservoirs: What Does the Atmosphere See?, *Ecosystems*, 21(5), 1058–1071, doi:10.1007/s10021-017-0198-9, 2018.
- Pu, J., Li, J., Zhang, T., Martin, J. B. and Yuan, D.: Varying thermal structure controls the dynamics of CO₂ emissions from a subtropical reservoir, south China, *Water Res.*, 115831, doi:10.1016/j.watres.2020.115831, 2020.
- R Core Team: R: A language and environment for statistical computing, [online] Available from: <https://www.r-project.org/>, 2017.
- 700 Rasilo, T., Hutchins, R. H. S., Ruiz-González, C. and del Giorgio, P. A.: Transport and transformation of soil-derived CO₂, CH₄ and DOC sustain CO₂ supersaturation in small boreal streams, *Sci. Total Environ.*, 579, 902–912, doi:10.1016/j.scitotenv.2016.10.187, 2017.
- 705 Raymond, P. A., Hartmann, J., Lauerwald, R., Sobek, S., McDonald, C., Hoover, M., Butman, D., Striegl, R., Mayorga, E., Humborg, C., Kortelainen, P., Dürr, H., Meybeck, M., Ciais, P. and Guth, P.: Global carbon dioxide emissions from inland waters, *Nature*, 503(7476), 355–359, doi:10.1038/nature12760, 2013.
- Reis, P. C. J., Thottathil, S. D., Ruiz-González, C. and Prairie, Y. T.: Niche separation within aerobic methanotrophic bacteria across lakes and its link to methane oxidation rates, *Environ. Microbiol.*, 22(2), 738–751, doi:10.1111/1462-2920.14877, 2020.
- 710 Roland, F., Vidal, L. O., Pacheco, F. S., Barros, N. O., Assireu, A., Ometto, J. P. H. B., Cimleris, A. C. P. and Cole, J. J.: Variability of carbon dioxide flux from tropical (Cerrado) hydroelectric reservoirs, *Aquat. Sci.*, 72(3), 283–293, doi:10.1007/s00027-010-0140-0, 2010.
- Rudorff, C. M., Melack, J. M., MacIntyre, S., Barbosa, C. C. F. and Novo, E. M. L. M.: Seasonal and spatial variability of CO₂ emission from a large floodplain lake in the lower Amazon, *J. Geophys. Res. Biogeosciences*, 116(4), 1–12, doi:10.1029/2011JG001699, 2011.
- 715 Sand-Jensen, K. and Staehr, P. A.: Net heterotrophy in small danish lakes: A widespread feature over gradients in trophic status and land cover, *Ecosystems*, 12(2), 336–348, doi:10.1007/s10021-008-9226-0, 2009.

- 720 Schmid, M., De Batist, M., Granin, N. G., Kapitanov, V. A., McGinnis, D. F., Mizandrontsev, I. B., Obzhairov, A. I. and Wüest, A.: Sources and sinks of methane in Lake Baikal: A synthesis of measurements and modeling, *Limnol. Oceanogr.*, 52(5), 1824–1837, doi:10.4319/lo.2007.52.5.1824, 2007.
- 725 Solomon, C. T., Bruesewitz, D. A., Richardson, D. C., Rose, K. C., Van de Bogert, M. C., Hanson, P. C., Kratz, T. K., Larget, B., Adrian, R., Leroux Babin, B., Chiu, C. Y., Hamilton, D. P., Gaiser, E. E., Hendricks, S., Istvá, V., Laas, A., O'Donnell, D. M., Pace, M. L., Ryder, E., Staehr, P. A., Torgersen, T., Vanni, M. J., Weathers, K. C. and Zhu, G.: Ecosystem respiration: Drivers of daily variability and background respiration in lakes around the globe, *Limnol. Oceanogr.*, 58(3), 849–866, doi:10.4319/lo.2013.58.3.0849, 2013.
- Soued, C. and Prairie, Y. T.: The carbon footprint of a Malaysian tropical reservoir: measured versus modelled estimates highlight the underestimated key role of downstream processes, *Biogeosciences*, 17(2), 515–527, doi:10.5194/bg-17-515-2020, 2020.
- 730 Staehr, P. A. and Sand-Jensen, K.: Temporal dynamics and regulation of lake metabolism, *Limnol. Oceanogr.*, 52(1), 108–120, doi:10.4319/lo.2007.52.1.0108, 2007.
- Tan, A. C.: Water and sediment quality of Batang Ai Reservoir. [online] Available from: <https://ir.unimas.my/id/eprint/10428/>, 2015.
- Tang, K. W., McGinnis, D. F., Frindte, K., Brüchert, V. and Grossart, H. P.: Paradox reconsidered: Methane oversaturation in well-oxygenated lake waters, *Limnol. Oceanogr.*, 59(1), 275–284, doi:10.4319/lo.2014.59.1.0275, 2014.
- 735 Tank, J. L., Rosi-Marshall, E. J., Griffiths, N. A., Entrekin, S. A. and Stephen, M. L.: A review of allochthonous organic matter dynamics and metabolism in streams, *J. North Am. Benthol. Soc.*, 29(1), 118–146, doi:10.1899/08-170.1, 2010.
- Teodoru, C. R., Prairie, Y. T. and del Giorgio, P. A.: Spatial Heterogeneity of Surface CO₂ Fluxes in a Newly Created Eastmain-1 Reservoir in Northern Quebec, Canada, *Ecosystems*, 14(1), 28–46, doi:10.1007/s10021-010-9393-7, 2011.
- 740 Thornton, K. W., Kimmel, B. L. and Payne, F. E.: *Reservoir Limnology: Ecological Perspectives*, John Wiley & Sons, Inc., 1990.
- Thottathil, S. D., Reis, P. C. J., del Giorgio, P. A. and Prairie, Y. T.: The Extent and Regulation of Summer Methane Oxidation in Northern Lakes, *J. Geophys. Res. Biogeosciences*, 123(10), 3216–3230, doi:10.1029/2018JG004464, 2018.

- Thottathil, S. D., Reis, P. C. J. and Prairie, Y. T.: Methane oxidation kinetics in northern freshwater lakes, *Biogeochemistry*, 143(1), 105–116, doi:10.1007/s10533-019-00552-x, 2019.
- 745 Tranvik, L. J., Cole, J. J. and Prairie, Y. T.: The study of carbon in inland waters-from isolated ecosystems to players in the global carbon cycle, *Limnol. Oceanogr. Lett.*, 3(3), 41–48, doi:10.1002/lol2.10068, 2018.
- Vachon, D. and del Giorgio, P. A.: Whole-Lake CO₂ Dynamics in Response to Storm Events in Two Morphologically Different Lakes, *Ecosystems*, 17(8), 1338–1353, doi:10.1007/s10021-014-9799-8, 2014.
- 750 Vachon, D., Langenegger, T., Donis, D. and McGinnis, D. F.: Influence of water column stratification and mixing patterns on the fate of methane produced in deep sediments of a small eutrophic lake, *Limnol. Oceanogr.*, 64(5), 2114–2128, doi:10.1002/lno.11172, 2019.
- Vachon, D., Sadro, S., Bogard, M. J., Lapierre, J., Baulch, H. M., Rusak, J. A., Denfeld, B. A., Laas, A., Klaus, M., Karlsson, J., Weyhenmeyer, G. A. and Giorgio, P. A.: Paired O₂–CO₂ measurements provide emergent insights into aquatic ecosystem function, *Limnol. Oceanogr. Lett.*, doi:10.1002/lol2.10135, 2020.
- 755 Venkiteswaran, J. J., Schiff, S. L., St. Louis, V. L., Matthews, C. J. D., Boudreau, N. M., Joyce, E. M., Beaty, K. G. and Bodaly, R. A.: Processes affecting greenhouse gas production in experimental boreal reservoirs, *Global Biogeochem. Cycles*, 27(2), 567–577, doi:10.1002/gbc.20046, 2013.
- 760 Wang, Q., Dore, J. E. and McDermott, T. R.: Methylphosphonate metabolism by *Pseudomonas* sp. populations contributes to the methane oversaturation paradox in an oxic freshwater lake, *Environ. Microbiol.*, 19(6), 2366–2378, doi:10.1111/1462-2920.13747, 2017.
- Wilkinson, G. M., Buelo, C. D., Cole, J. J. and Pace, M. L.: Exogenously produced CO₂ doubles the CO₂ efflux from three north temperate lakes, *Geophys. Res. Lett.*, 43(5), 1996–2003, doi:10.1002/2016GL067732, 2016.
- Williams, P. J. I. and Robertson, J. E.: Overall planktonic oxygen and carbon dioxide metabolisms: the problem of reconciling observations and calculations of photosynthetic quotients, *J. Plankton Res.*, doi:10.1093/oxfordjournals.plankt.a042366, 1991.
- 765 Winslow, L., Read, J., Woolway, R., Brenttrup, J., Leach, T., Zwart, J., Albers, S. and Collinge, D.: rLakeAnalyzer: Lake Physics Tools, [online] Available from: <https://cran.r-project.org/package=rLakeAnalyzer>, 2018.
- Wüest, A. and Lorke, A.: Small-Scale Turbulence and Mixing: Energy Fluxes in Stratified Lakes, in *Encyclopedia of Inland Waters*, pp. 628–635, Elsevier., 2009.
- Yao, M., Henny, C. and Maresca, J. A.: Freshwater Bacteria Release Methane as a By-Product of Phosphorus Acquisition,

770 edited by J. E. Kostka, *Appl. Environ. Microbiol.*, 82(23), 6994–7003, doi:10.1128/AEM.02399-16, 2016.

Zarfl, C., Lumsdon, A. E., Berlekamp, J., Tydecks, L. and Tockner, K.: A global boom in hydropower dam construction, *Aquat. Sci.*, 77(1), 161–170, doi:10.1007/s00027-014-0377-0, 2015.

Zhang, Q., Tao, Z., Ma, Z., Gao, Q., Deng, H., Xu, P., Ding, J., Wang, Z. and Lin, Y.: Hydro-ecological controls on riverine organic carbon dynamics in the tropical monsoon region, *Sci. Rep.*, 9(1), 1–11, doi:10.1038/s41598-019-48208-y, 2019.

775

Table 1: Mean (\pm SD) of physical and chemical variables measured at the surface of the three reservoir sections.

Variables	Units	Inflows	Branches	Main basin
z_{epi}	m	1.3 (\pm 1.6)	8 (\pm 2.3)	10.6 (\pm 1.7)
Secchi	m	1.2 (\pm 0.9)	5.1 (\pm 1.2)	5.5 (\pm 1.2)
Temperature	$^{\circ}$ C	27.1 (\pm 2.5)	30.7 (\pm 0.5)	30.6 (\pm 0.5)
pH		6.5 (\pm 0.3)	7.2 (\pm 0.2)	7.2 (\pm 0.2)
O ₂	%	94.9 (\pm 7.7)	102.7 (\pm 4.5)	99.3 (\pm 4.8)
DOC	mg L ⁻¹	0.8 (\pm 0.4)	0.9 (\pm 0.2)	0.9 (\pm 0.2)
TP	μ g L ⁻¹	20.7 (\pm 7.6)	6.2 (\pm 1.7)	5.8 (\pm 2.6)
TN	mg L ⁻¹	0.14 (\pm 0.04)	0.12 (\pm 0.04)	0.1 (\pm 0.03)
Chla	μ g L ⁻¹	2.1 (\pm 1.7)	1.7 (\pm 1)	1.2 (\pm 0.5)

780

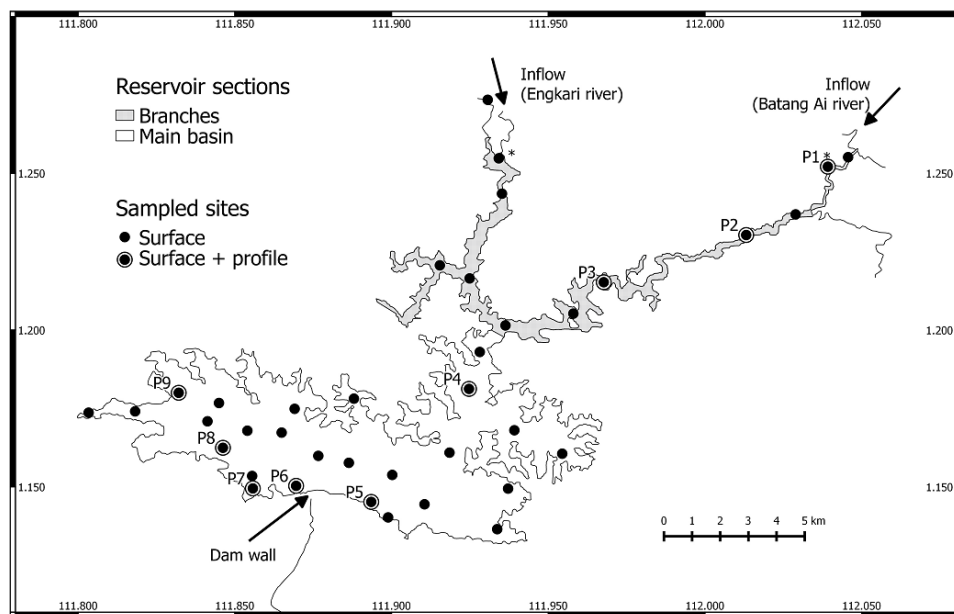
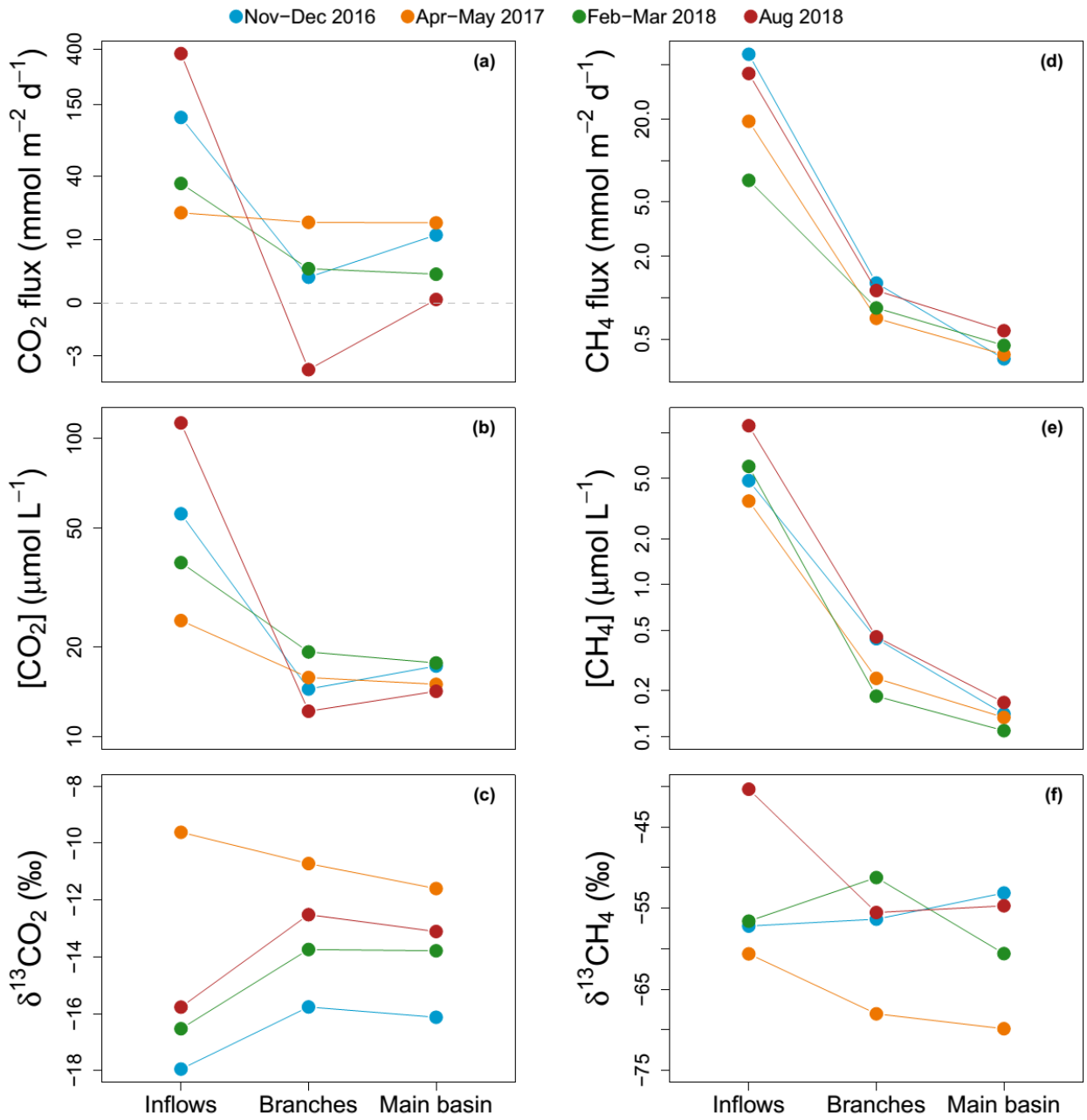
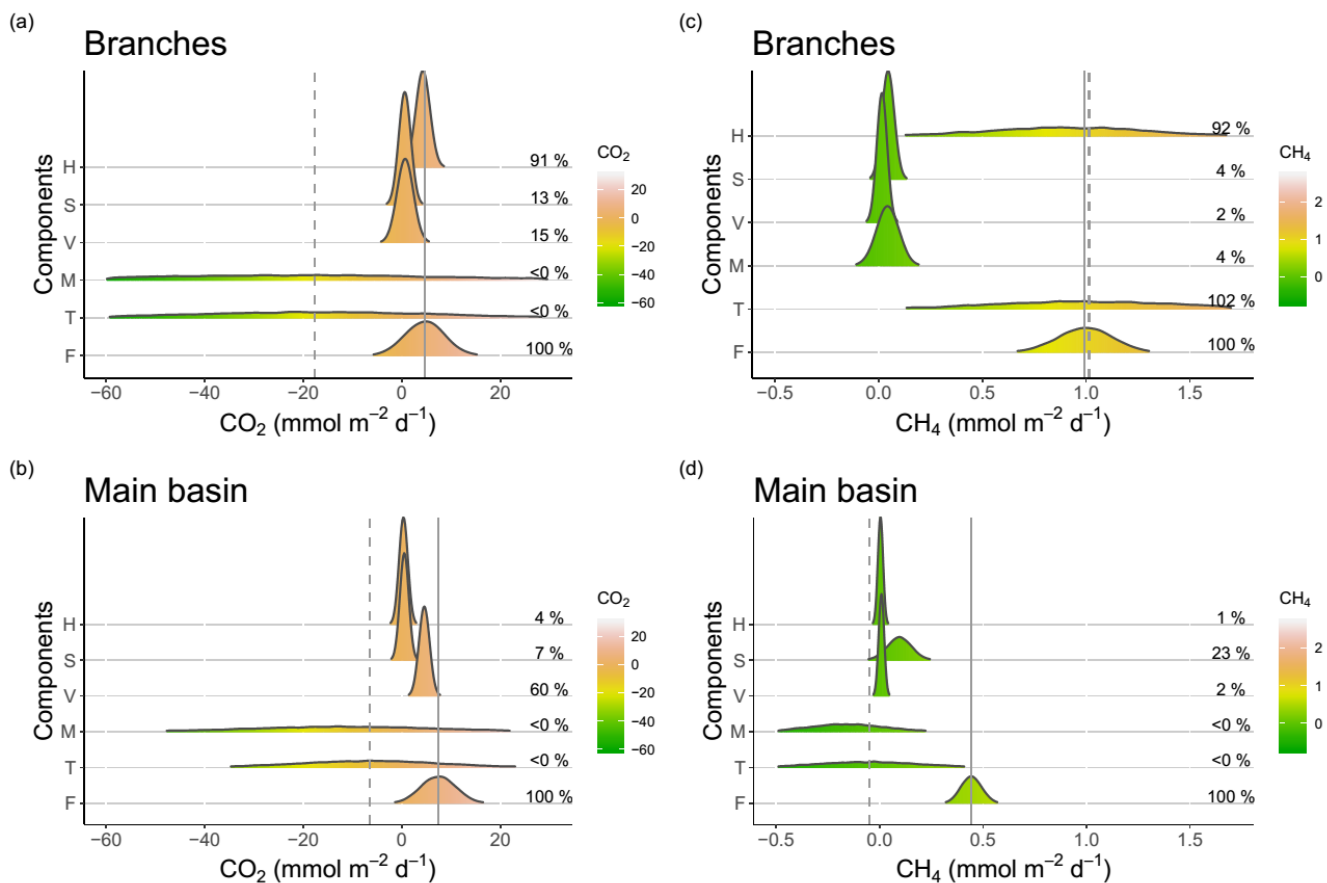


Figure 1: Map of Batang Ai reservoir with delimited sections (branches and main basin) and sampling points. * Represents sampling points at the branches extremities.

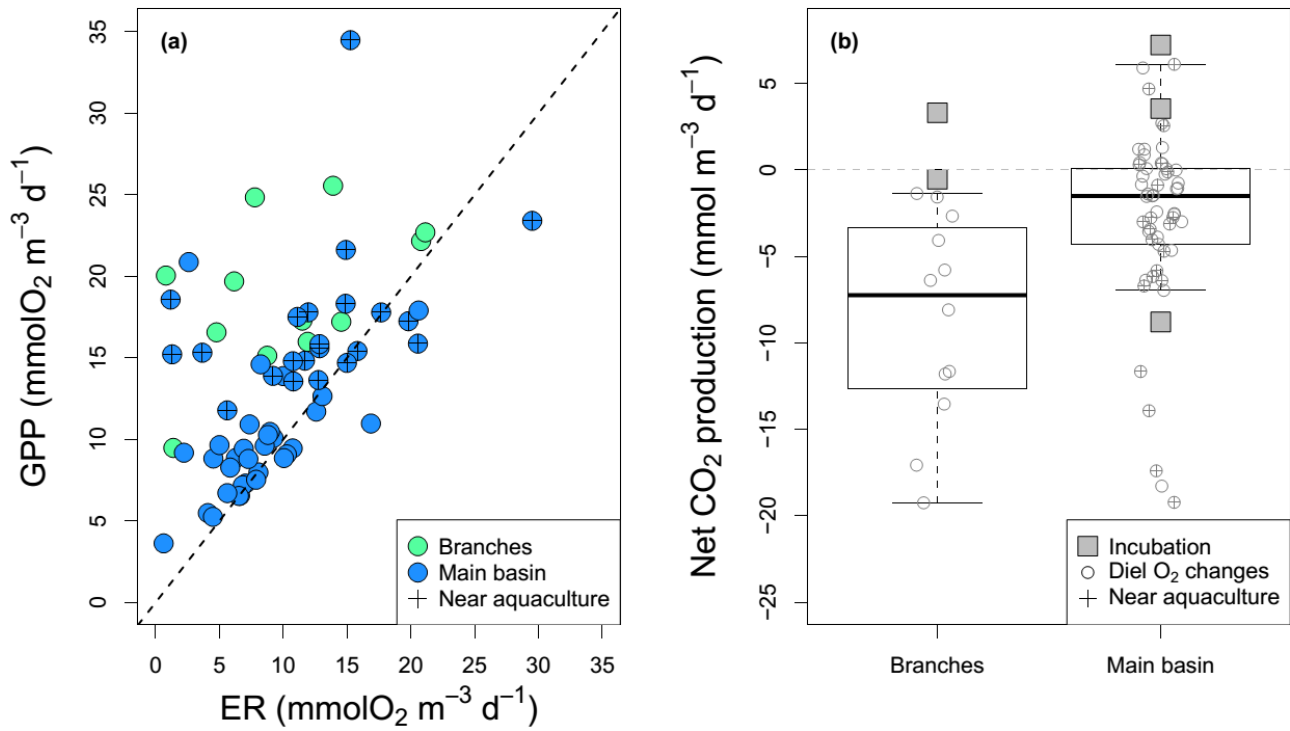


785 **Figure 2: Average of spatially interpolated surface CO₂ (a, b, c) and CH₄ (d, e, f) fluxes (a, d), concentrations (b, e), and isotopic signatures (c, f) along the hydrological continuum from the reservoir inflows to the main basin for each sampling campaign.**

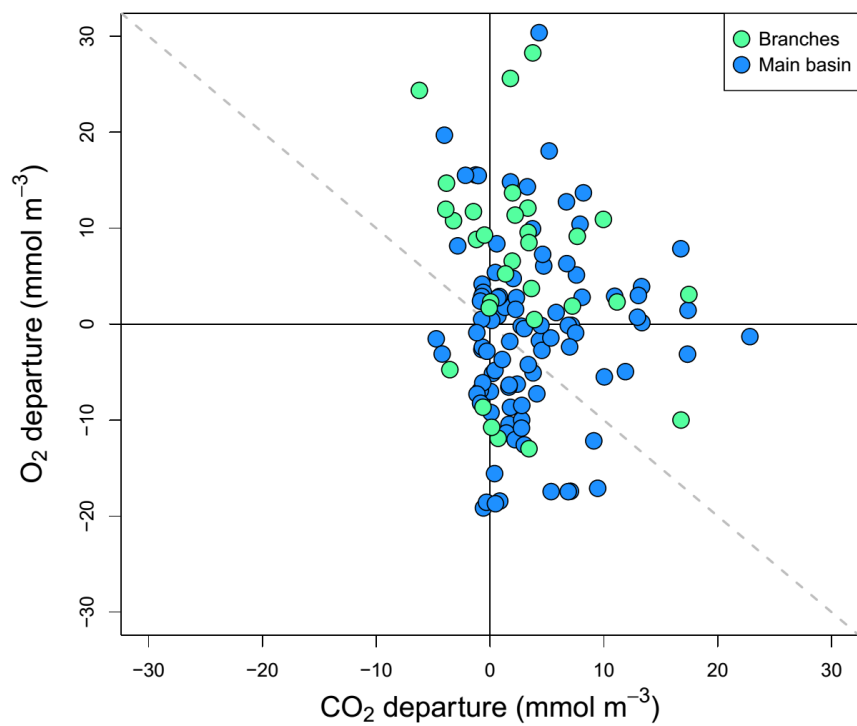


790 **Figure 3: Density distributions of the different components of CO₂ (a, b) and CH₄ (c, d) surface budgets in the reservoir branches (a, c) and main basin (b, d). Components are: H = horizontal flow inputs, S = sediment inputs, V = vertical inputs, M = net metabolism (average of the incubation and diel O₂ monitoring methods), T = sum of all estimated sources and processes in the surface layer, and F = measured surface fluxes. Density curves are based on simulated normal distributions using the mean and standard error of each component. The x-axes and color scales represent the areal rate of CO₂ / CH₄. Mean values of the fraction of each component (in %) relative to the mean surface flux (F) are reported on the right side in each panel. The solid and dashed grey lines represent the means of F and T respectively.**

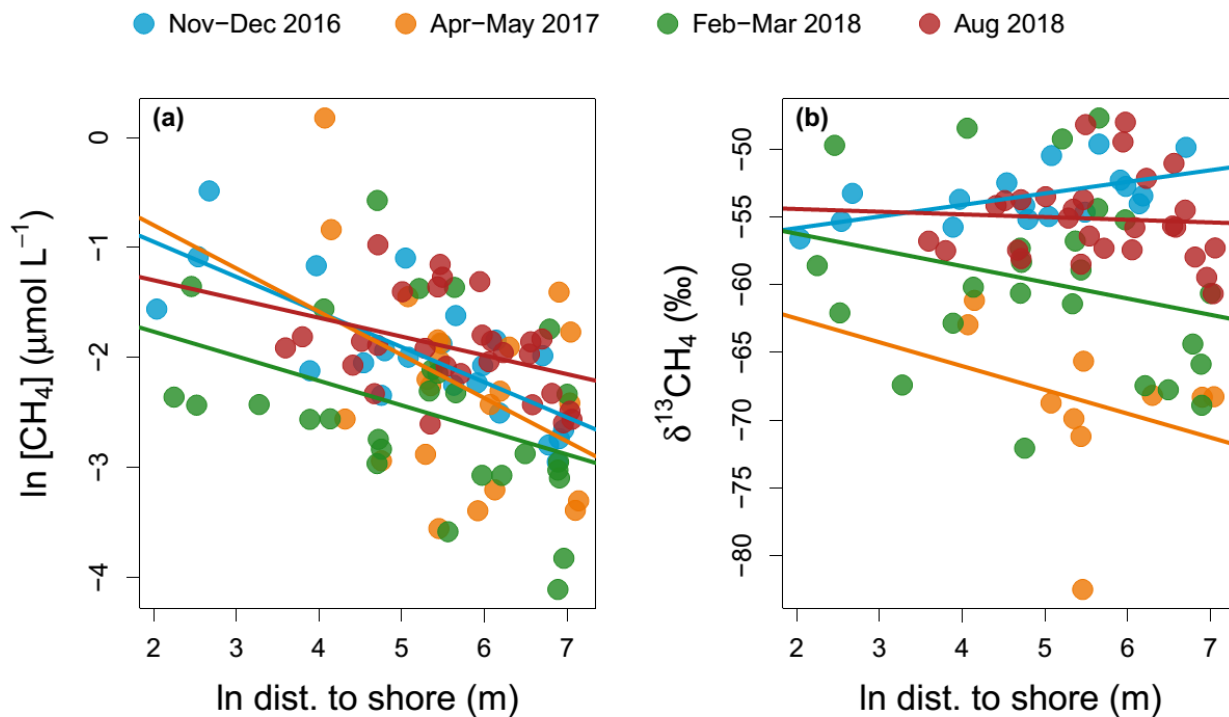
795



800 **Figure 4: Epilimnetic daily GPP versus ER rates (a) derived from diel O_2 changes in the reservoir branches and main basin (including sites near aquacultures), with the 1:1 line (dotted). Panel (b) shows boxplots of the corresponding rates of CO_2 NEP in the branches and main basin, with boxes bounds, whiskers, solid line, and open circles, and squares representing the 25th and 75th percentiles, the 10th and 90th percentiles, the median, single data points (diel O_2 method), and incubation derived rates respectively.**



805 **Figure 5: Surface O₂ versus CO₂ departure from saturation for all sampled surface sites in the reservoir main basin and branches across all sampling campaigns.**



810 **Figure 6: Regression of CH₄ concentration (a) and isotopic signature (b) as a function of distance to shore in each sampling campaign in the main reservoir basin. For CH₄ concentration, regressions lines have the following statistics in order of sampling: p-values: < 0.001, 0.06, 0.03, 0.05, and R²_{adj}: 0.54, 0.13, 0.11. For δ¹³CH₄, all regressions had p-values > 0.2 except for the Nov-Dec 2016 campaign with p-value = 0.01 and R²_{adj} = 0.29.**